Hydrometeor Mixing Ratio Retrievals for Storm-Scale Radar Data Assimilation: Utility of Current Relations and Potential Benefits of Polarimetry

JACOB T. CARLIN, ALEXANDER V. RYZHKOV, AND JEFFREY C. SNYDER

Cooperative Institute for Mesoscale Meteorological Studies, University of Oklahoma, and NOAA/OAR/National Severe Storms Laboratory, Norman, Oklahoma

ALEXANDER KHAIN

The Hebrew University of Jerusalem, Jerusalem, Israel

(Manuscript received 8 December 2015, in final form 9 May 2016)

ABSTRACT

The assimilation of radar data into storm-scale numerical weather prediction models has been shown to be beneficial for successfully modeling convective storms. Because of the difficulty of directly assimilating reflectivity (Z), hydrometeor mixing ratios, and sometimes rainfall rate, are often retrieved from Z observations using retrieval relations, and are assimilated as state variables. The most limiting (although widely employed) cases of these relations are derived, and their assumptions and limitations are discussed.

To investigate the utility of these retrieval relations for liquid water content (LWC) and ice water content (IWC) in rain and hail as well as the potential for improvement using polarimetric variables, two models with spectral bin microphysics coupled with a polarimetric radar operator are used: a one-dimensional melting hail model and the two-dimensional Hebrew University Cloud Model. The relationship between LWC and Z in pure rain varies spatially and temporally, with biases clearly seen using the normalized number concentration. Retrievals using Z perform the poorest while specific attenuation and specific differential phase shift (K_{DP}) perform much better. Within rain–hail mixtures, separate estimation of LWC and IWC is necessary. Prohibitively large errors in the retrieved LWC may result when using Z. The quantity K_{DP} can be used to effectively retrieve the LWC and to isolate the contribution of IWC to Z. It is found that the relationship between Z and IWC is a function of radar wavelength, maximum hail diameter, and principally the height below the melting layer, which must be accounted for in order to achieve accurate retrievals.

1. Introduction

The prospect of explicitly modeling and predicting convection is relatively recent, only beginning to be explored within the past 25 years (Droegemeier 1990; Lilly 1990). Lilly (1990) cited the upcoming Weather Surveillance Radar-1988 Doppler (WSR-88D) radar network, which would be deployed and operational over the next few years, as the key observing system toward making this possible. Doppler radar is the only source of data of sufficient spatial and temporal resolution to fully resolve convective systems in time and space, and as such is one of the primary sources of information for assimilation when modeling convection. Many studies have shown that the assimilation of radar reflectivity factor, hereafter reflectivity (Z), in conjunction with radial velocity (V_r), can help reduce the spinup time for storms (e.g., Xue et al. 2003; Dawson and Xue 2006; Hu et al. 2006a; Dowell et al. 2011; Gao and Stensrud 2012) and has the potential to provide a positive impact on subsequent forecasts (e.g., Tong and Xue 2005; Dawson and Xue 2006; Hu et al. 2006a,b; Gao and Stensrud 2012; Xue et al. 2013).

Owing to recent developments and successes in convective-scale modeling (i.e., on the order of a few kilometers or less), the National Severe Storms Laboratory in Norman, Oklahoma, is leading the development of a Warn-on-Forecast paradigm (Stensrud et al. 2009, 2013), requiring the use of high-resolution,

Corresponding author address: Jacob T. Carlin, CIMMS/NSSL, National Weather Center, 120 David L. Boren Blvd., Norman, OK 73072.
E-mail: jacob.carlin@noaa.gov

DOI: 10.1175/MWR-D-15-0423.1

convection-resolving models that can rapidly assimilate radar data and be used in real time. As such, efficient and effective assimilation of radar data is an emerging research frontier.

While the assimilation of V_r into models is relatively well established (e.g., Gao et al. 2004), developing an optimal method for utilizing Z in models remains comparatively challenging. In addition to issues regarding data quality control and uncertain error statistics, a primary source of uncertainty in the assimilation of Z is the need to link Z and model state variables so that a direct comparison can be drawn and the assimilation process can occur. Two paradigms currently exist for doing this: retrievals and forward operators.

Forward operators are used to convert model variables to observed ones in order to form observation increments. Many observation operators of varying complexity exist for calculating simulated radar variables from hydrometeor mixing ratios (q) and the parameters of model-predicted particle size distributions (PSDs) (e.g., Smith et al. 1975; Tong and Xue 2005; Jung et al. 2008; Ryzhkov et al. 2011). These operators are used by assimilation methods including the ensemble Kalman filter (EnKF; Evensen 1994), which has gained increasing attention in recent years due to its success in effectively assimilating radar data and forming accurate storm-scale analyses (e.g., Tong and Xue 2005; Xue et al. 2006; Aksoy et al. 2009; Dowell et al. 2011; Dawson et al. 2012; Jung et al. 2012), as well as some implementations of variational methods (e.g., Gao and Stensrud 2012). In contrast, retrievals refer to the process of obtaining unobserved variables from observed variables. For Z, this means retrieving either rainfall rate (R) for quantitative precipitation estimation applications or, more typically for assimilation, q. This method is currently used by many "cloud analysis" systems, such as the Advanced Regional Prediction System's (ARPS; Xue et al. 2003) Cloud Analysis (e.g., Zhang et al. 1998; Zhang 1999; Brewster 2002; Hu et al. 2006a), and in some variational methods in which the minimization of the cost function is found with respect to a hydrometeor control variable (e.g., Sun and Crook 1998; Wu et al. 2000; Xiao and Sun 2007).

Forward operators have the advantage of having model-predicted microphysical parameters to use in the calculation of Z, which, given an accurate forward operator, should provide a reliable estimate of model Z (although improving upon forward operators is itself an active area of ongoing research). Retrievals present a more difficult problem as nonlinearity in the forward operator for Z may result in a nonunique solution of the retrieved microphysical parameters. As such, various assumptions (discussed further in section 2) may be required to constrain the problem in order to retrieve q from a single measurement of Z. However, despite these limitations, positive impacts from using retrievals to assimilate Z have been found in the form of reduced spinup time and forecast error (e.g., Souto et al. 2003; Dawson and Xue 2006; Hu et al. 2006a; Zhao and Xue 2009; Schenkman et al. 2011a). These improvements, together with computational efficiency, have resulted in the continuing widespread use of retrieval equations in modeling and radar assimilation studies (e.g., Hu and Xue 2007; Kain et al. 2010; Stensrud and Gao 2010; Schenkman et al. 2011b; Xue et al. 2014; Dawson et al. 2015; Chang et al. 2016). Given their ubiquity but potential issues, the primary focus of this paper will be examining the utility and consequences of employing retrieval equations under the most restrictive assumptions.

The summer of 2013 saw the completion of the dual-polarization upgrade for the national WSR-88D radar network. Radar polarimetry capitalizes on the principle that nonspherical particles scatter incoming electromagnetic energy differently for different polarization planes, from which information about scatterer characteristics can be inferred. The benefits of polarimetry are wide reaching and include updraft detection (Brandes et al. 1995; Kumjian and Ryzhkov 2008; Picca et al. 2010; Kumjian et al. 2012, 2014; Snyder et al. 2015), improved rainfall estimation (Ryzhkov et al. 2005b), and hydrometeor classification algorithms (HCAs; Lim et al. 2005; Park et al. 2009; Snyder et al. 2010; Al-Sakka et al. 2013; Thompson et al. 2014), which generally employ fuzzy-logic qualifiers (Liu and Chandrasekar 2000; Straka et al. 2000). Unfortunately, despite these benefits, the modeling community has yet to truly capitalize on the availability of polarimetric radar data.

Among the variables that polarimetry offers are the differential reflectivity (Z_{DR}) and specific differential phase shift (K_{DP}). The quantity Z_{DR} (dB) is the logarithmic ratio of the backscattered power at the horizontal and vertical polarizations (Seliga and Bringi 1976) with a value of 0 dB for isotropic scatterers and, generally, positive values for oblate particles. The quantity Z_{DR} is 1) sensitive to hydrometeor orientation, composition, and density; 2) unaffected by hydrometeor concentration; and 3) proportional to the median particle size in a volume for particles with axis ratios that vary as a function of size, such as raindrops (which become increasingly oblate with size; e.g., Thurai et al. 2009). The quantity K_{DP} (degrees per kilometer) measures the rate at which a phase difference accumulates between the horizontally and vertically polarized waves due to the slowing of the horizontally polarized wave relative to the vertically polarized wave in anisotropic

particles such as raindrops. It is immune to isotropic scatterers and has been explored extensively for mitigating hail contamination in quantitative precipitation estimation (e.g., Balakrishnan and Zrnić 1990; Aydin et al. 1995). For a further review of radar polarimetry, see Doviak and Zrnić (1993), Zrnić and Ryzhkov (1999), and Kumjian (2013a,b,c).

In addition to the variables directly measured, dual-polarization data can be used to estimate specific attenuation at horizontal polarization, A_H, which is difficult to do using single-polarization radars. Specific attenuation is the rate at which power is lost from the emitted wave and is particularly attractive for the estimation of both the rain mixing ratio (q_r) and R as it is a lower-order moment of the drop size distribution (DSD) than Z and therefore much less sensitive to variability of the DSD. The quantity A_H is also independent of radar miscalibration and partial beam blockage (Ryzhkov et al. 2014).

Improved estimates of R over the traditional use of $R(Z)$ is one of the primary benefits of polarimetry and has already seen much use. A multitude of polarimetric relations for estimating R have been described throughout the literature, including $R(Z, Z_{DR})$ (e.g., Seliga and Bringi 1976; Seliga et al. 1981), $R(K_{DP})$ (e.g., Ryzhkov et al. 2005a; Cifelli et al. 2011), $R(Z, N_w)$ (Testud et al. 2001; Tabary et al. 2011), and, more recently, $R(A_H)$ (Ryzhkov et al. 2014). The normalized drop concentration N_w (Testud et al. 2001) is given by

$$N_w = \frac{4^4}{\pi \rho_w} \frac{\mathrm{LWC}}{D_m^4}, \tag{1}$$

where D_m is the volume-weighted mean diameter (equal to the ratio of the fourth to the third moment of the DSD) and LWC is the liquid water content. The quantity N_w represents the intercept parameter for an exponential size distribution with an equivalent D_m and LWC *regardless of actual DSD shape*. For the case of the Marshall–Palmer DSD (in which $N_w = N_{0r}$), $\log_{10} N_w \approx 3.9$. Tropical rain with DSDs skewed toward smaller drops features high values of N_w whereas rain from strong continental convection with DSDs skewed toward larger drops features low values of N_w (Bringi et al. 2003).

Although polarimetric R retrievals have successfully improved upon $R(Z)$ retrievals, the need for similar, more sophisticated relations for retrieving LWC and ice water content (IWC) for assimilation still exists. Little work has been done in assimilating hydrometeor retrievals using dual-polarization data. Wu et al. (2000) attempted to use Z_{DR} to help partition Z for retrieving q_r and q_h, but found difficulty in achieving an accurate forecast, presumably due to insufficient microphysics. More recently, Li and Mecikalski (2010), using single-moment warm rain microphysics, examined the impact of assimilating $q_r(Z, Z_{DR})$ using a relation derived from Ulbrich and Atlas (1984) and found a positive impact on the resultant forecast. In a follow-up study, the assimilation of $q_r(Z)$ was compared to that of both $q_r(Z, Z_{DR})$ and $q_r(Z_{DR}, K_{DP})$ using relations from Bringi and Chandrasekar (2001). It was found that assimilating $q_r(Z_{DR}, K_{DP})$ resulted in the best forecast, highlighting the potential benefits of assimilating polarimetric data.

This paper will use numerical models to examine the utility of the most simplified version of commonly used retrieval equations for rain and hail and the potential for both spectral bin microphysics and polarimetry to offer improvements for those cases. Section 2 will provide a review of the current retrieval equations and their implicit assumptions. Alternative relations for retrieving R and q_r will be discussed in section 3. Section 4 will describe the two spectral bin microphysics models used in this study. The evolution in space and time of retrieved rain biases will be presented in section 5, while the separate estimation of rain and hail in rain–hail mixtures will be examined in section 6. Section 7 will provide a summary of conclusions as well as a discussion of future work.

2. Summary of existing retrieval equations

The mixing ratio of hydrometeor x, q_x, is proportional to the third moment of the size distribution and is given by

$$q_x = \frac{\rho_x}{\rho} \frac{\pi}{6} \int_0^\infty D^3 N(D)\, dD, \tag{2}$$

where ρ is the air density, ρ_x is the hydrometeor density, D is the particle equivalent spherical diameter, and $N(D)$ is the particle size distribution of x. The rainfall rate (flux) R expressed in mm h^{-1}, is given by

$$R = 6\pi \times 10^{-4} \int_0^\infty D^3 v(D) N(D)\, dD. \tag{3}$$

If using the relation for raindrop fall speed, $v(D)$, proposed by Atlas and Ulbrich (1977),

$$v = 3.778 D^{0.67} \tag{4}$$

it is seen that R is proportional to the 3.67th moment of the size distribution.

The radar reflectivity factor is defined most generally as

$$Z = \frac{\lambda^4}{\pi^5 |K_w|^2} \int_0^\infty \sigma(D) N(D)\, dD, \tag{5}$$

where λ is the radar wavelength, $|K_w|^2$ ($\approx$0.93) is the squared dielectric factor related to the dielectric constant for water ε_w by

$$|K_w|^2 = \left| \frac{(\varepsilon_w - 1)}{(\varepsilon_w + 2)} \right|^2, \tag{6}$$

and $\sigma(D)$ is the radar cross section of a particle of size D, given by

$$\sigma(D) = 4\pi |s(D)|^2, \tag{7}$$

where $s(D)$ is the backscattering amplitude of a particle of size D. For the special case where particles are assumed to be spherical and the resonance parameter $\Re$, given by

$$\Re = \frac{D\sqrt{|\varepsilon|}}{\lambda}, \tag{8}$$

is less than approximately 0.3–0.4, the Rayleigh approximation can be invoked. In this approximation, the backscattering amplitude of a particle is equal to

$$s(D) = \frac{1}{2} \frac{\pi^2 D^3}{\lambda^2} \frac{(\varepsilon_x - 1)}{(\varepsilon_x + 2)} \tag{9}$$

so that the radar reflectivity for rain is equal to

$$Z = \int_0^\infty D^6 N(D)\, dD \tag{10}$$

or, more generally for hydrometeor species x,

$$Z_x = \frac{|K_x|^2}{|K_w|^2} \int_0^\infty D^6 N(D)\, dD. \tag{11}$$

For most existing retrieval equations, as in most single- or double-moment bulk microphysics schemes, an exponential size distribution, described by

$$N_x(D) = N_{0x} \exp(-\Lambda_x D), \tag{12}$$

where N_{0x} is the intercept parameter and Λ_x is the slope parameter of x, is generally assumed for all hydrometeor species. Using this size distribution and employing the gamma function, Eq. (11) can be expressed as

$$Z_x = N_{0x} \frac{|K_x|^2}{|K_w|^2} \frac{\Gamma(7)}{\Lambda^7}, \tag{13}$$

where

$$\Lambda_x = \left(\frac{\rho_x \pi N_{0x}}{\rho q_x} \right)^{0.25}. \tag{14}$$

Substituting Eq. (14) into Eq. (13), the Z–q relation can be expressed most generally as

$$Z_x = \frac{7.2 \times 10^{20} \frac{|K_x^2|}{|K_w^2|} (\rho q_x)^{1.75}}{\pi^{1.75} N_{0x}^{0.75} \rho_x^{1.75}}, \tag{15}$$

where Z_x is in units of mm^6 m^{-3}.

Equation (15) is the general form of the forward operator equations used in many studies to calculate simulated Z (e.g., Tong and Xue 2005; Dowell et al. 2011) as well as for retrievals. Further assumptions are often made depending on the microphysics scheme being used. If double-moment microphysics are used, N_{0x} is allowed to vary, which significantly improves the utility of these equations for retrievals. In practice, the existing N_{0x} field from a previous model forecast can be used, potentially limiting further assumptions to only those pertaining to hydrometeor density and wetness. Additionally, a diagnosed N_{0x} from a constrained q_x–N_{0x} relation (Zhang et al. 2008) based on the results of simulations with double-moment microphysics can be used with single-moment microphysics and has recently been tested with the ARPS Cloud Analysis with encouraging results (Wainwright et al. 2014; Pan et al. 2016). However, for the typical case of single-moment microphysics, or during an initial assimilation cycle in which background estimates of N_{0x} are not available, N_{0x} is fixed at a constant value. It is these most limiting cases, and the consequences of the assumptions therein, that are investigated in this study and discussed below.

For rain, N_{0r} is usually assumed to be fixed at 8×10^6 m^{-4} (Marshall and Palmer 1948), ρ_r is equal to 1000 kg m^{-3}, and $K_r = K_w$, resulting in a retrieval equation for rain of

$$Z_r = 3.63 \times 10^9 (\rho q_r)^{1.75}. \tag{16}$$

For snow, different equations may be used if the snow is dry above the melting level or wet below the melting level. For dry snow, the dielectric constant must be modified from that of pure ice to account for its decreased density from the inclusion of air. Smith (1984) presents two formulations for this seen throughout the literature. In the first formulation (e.g., Tong and Xue 2005), the particle diameter represents that of dry snow and $|K_i|^2$ is equal to that for solid ice, 0.17, resulting in a dielectric factor of snow of

$$|K_s|^2 = |K_i|^2 \left(\frac{\rho_s^2}{\rho_i^2}\right). \quad (17)$$

In the second formulation (e.g., Dowell et al. 2011; Gao and Stensrud 2012), the particle diameter is the equivalent diameter of the particle if it were entirely melted. In this case, $|K_i|^2$ must be adjusted to account for this decreased diameter and instead takes the value 0.21, denoted by $|K_i^*|^2$. The dielectric factor of snow now becomes

$$|K_s|^2 = |K_i^*|^2 \left(\frac{\rho_s^2}{\rho_w^2}\right). \quad (18)$$

Assuming $\rho_s = 100\,\mathrm{kg\,m^{-3}}$ and $N_{0s} = 3 \times 10^6\,\mathrm{m^{-4}}$ (Gunn and Marshall 1958),

$$Z_s = 9.80 \times 10^8 (\rho q_s)^{1.75} \quad (\text{for} \quad T \le 0°\text{C}). \quad (19)$$

For melting snow, the surface of the snow is assumed to be wet with $|K_s|^2 = |K_w|^2$. Otherwise, following a similar procedure as dry snow,

$$Z_s = 4.26 \times 10^{11} (\rho q_s)^{1.75} \quad (\text{for} \quad T > 0°\text{C}). \quad (20)$$

Finally, for hail, it is commonly assumed that $N_{0h} = 4 \times 10^4\,\mathrm{m^{-4}}$ (Federer and Waldvogel 1975), $\rho_h = 900\,\mathrm{kg\,m^{-3}}$, and with $|K_h|^2$ adjusted in an analogous manner to Eq. (18). This results in the retrieval equation for (dry) hail of

$$Z_h = 4.33 \times 10^{10} (\rho q_h)^{1.75}. \quad (21)$$

This set of simplified retrieval equations exhibit limitations of varying validity due to the assumptions made in deriving them. The most restrictive assumption is fixing N_{0x} to be constant for the presumed exponential size distributions of all species. For rain, Kessler (1969) described this assumption as one that "does some violence to the physics of the evaporation process," and Sun (2005) noted that it is "not trivial to quantify" the error induced by such an assumption. Any canting with respect to vertical that particles may experience is neglected. The assumption of constant density may be a poor one for ice hydrometeors, particularly for ρ_s, which generally varies nearly inversely with diameter with a mass–diameter relation for snow having a diameter exponent closer to 2 than 3 (e.g., Brandes et al. 2007), resulting in an approximate D^4 dependence for Z from snow rather than a D^6 dependence. The density of hail and graupel may also vary from that of pure ice as they may be spongy and contain air cavities, and may be either wet or dry below the melting layer depending on whether meltwater seeps inside to fill the voids (Dowell et al. 2011). Additionally, by invoking the Rayleigh approximation, resonance scattering from large hydrometeors is neglected and subsequently any dependence on radar wavelength or nonsphericity is excluded. However, it should be noted that efforts have been made in some studies (e.g., Dowell et al. 2011) to approximate the effects of resonance scattering by exponentiating a modified retrieval equation for wet hail to 0.95, based on the work of Smith et al. (1975) and given by

$$Z_h = \left[\frac{7.2 \times 10^{20} (\rho q_h)^{1.75}}{\pi^{1.75} N_{0h}^{0.75} \rho_h^{1.75}}\right]^{0.95} = 6.13 \times 10^{10} (\rho q_h)^{1.6625}. \quad (22)$$

Hereafter, the phrase "legacy retrieval equations" will specifically refer to this set of simplified equations.

Implementing the legacy retrieval equations may require additional assumptions. Typically, the radar data are first interpolated to the model grid and quality controlled. If mixed-phase microphysics are being used, the problem of determining which species to retrieve is underdetermined for volumes with multiple species and only one Z measurement. To combat this, the existing background species can be used or, in the absence of any background species (e.g., in a noncycling mode), hydrometeor species can be determined based on empirical observations using temperature (e.g., to differentiate rain and snow) and Z (e.g., for identifying hail) thresholds. Once the dominant species has been established, multiple species may also be retrieved by partitioning the Z according to empirical rules involving environmental variables (e.g., a linear ramp from wet snow to rain between 0° and 5°C). The q for each species is then retrieved from Z using equations such as Eqs. (16), (19), (20), and (21), and can be directly inserted (as in the ARPS Cloud Analysis, predicated on the belief that radar observations are more accurate than the model predicted q) or assimilated variationally or otherwise.

In the following sections, LWC and IWC (both in $\mathrm{g\,m^{-3}}$) are used in place of q_r and q_h (and q_g, where noted) due to convention, differing only by a factor of ρ.

3. Alternative relations for rain

To investigate the use of dual-polarization data for improving LWC retrievals and to review the utility of polarimetric R relations, a large two-dimensional video disdrometer dataset from Oklahoma in pure rain was used. The data were collected over a 7-yr period in Oklahoma and contain 47 144 unique 1-min DSDs from both stratiform and convective rainfall. Following Ryzhkov et al. (2014), polarimetric radar variables at S ($\lambda = 11.0\,\mathrm{cm}$) and C band ($\lambda = 5.3\,\mathrm{cm}$) for each DSD

TABLE 1. Retrieval relations for LWC and R at both S- and C-band from disdrometer data, along with the root-mean-square error (RE), Pearson correlation coefficient (r), and standard deviation (σ) of each relation, where LWC is in g m^{-3}, R is in mm h^{-1}, Z is linear in units of mm^6 m^{-3}, Z_{DR} is linear and unitless, N_w is in m^{-3} mm^{-1}, K_{DP} is in ° km^{-1}, and A_H is in dB km^{-1}.

S band					C band				
No.	Relation	RE	r	σ	No.	Relation	RE	r	σ
	LWC observations	—	—	0.39		LWC observations	—	—	0.39
1	$\mathrm{LWC}(Z) = 1.74 \times 10^{-3} Z^{0.640}$	0.28	0.82	0.49	6	$\mathrm{LWC}(Z) = 1.59 \times 10^{-3} Z^{0.657}$	0.53	0.67	0.69
2	$\mathrm{LWC}(K_{DP}) = 2.24 K_{DP}^{0.725}$	0.17	0.91	0.41	7	$\mathrm{LWC}(K_{DP}) = 1.27 K_{DP}^{0.714}$	0.16	0.92	0.40
3	$\mathrm{LWC}(A_H) = 115 A_H^{0.917}$	0.13	0.96	0.43	8	$\mathrm{LWC}(A_H) = 11.0 A_H^{0.777}$	0.40	0.78	0.61
4	$\mathrm{LWC}(Z, Z_{DR}) = 1.33 \times 10^{-3} Z^{0.696} Z_{DR}^{-0.981}$	0.20	0.89	0.44	9	$\mathrm{LWC}(Z, Z_{DR}) = 1.29 \times 10^{-3} Z^{0.701} Z_{DR}^{-0.790}$	0.32	0.80	0.52
5	$\mathrm{LWC}(Z, N_w) = 1.16 \times 10^{-4} Z^{0.550} N_w^{0.411}$	0.05	0.99	0.40	10	$\mathrm{LWC}(Z, N_w) = 1.51 \times 10^{-4} Z^{0.572} N_w^{0.363}$	0.16	0.94	0.45
	R observations	—	—	8.36		R observations	—	—	8.36
11	$R(Z) = 1.94 \times 10^{-2} Z^{0.692}$	5.07	0.87	10.05	16	$R(Z) = 1.72 \times 10^{-2} Z^{0.714}$	11.69	0.68	15.60
12	$R(K_{DP}) = 46.9 K_{DP}^{0.794}$	2.67	0.95	8.59	17	$R(K_{DP}) = 25.0 K_{DP}^{0.777}$	2.46	0.96	8.30
13	$R(A_H) = 3380 A_H^{0.995}$	2.34	0.97	9.23	18	$R(A_H) = 243 A_H^{0.826}$	7.83	0.81	12.90
14	$R(Z, Z_{DR}) = 1.60 \times 10^{-2} Z^{0.738} Z_{DR}^{-0.912}$	3.33	0.93	8.80	19	$R(Z, Z_{DR}) = 1.63 \times 10^{-3} Z^{0.731} Z_{DR}^{-0.399}$	8.68	0.75	12.91
15	$R(Z, N_w) = 2.68 \times 10^{-3} Z^{0.638} N_w^{0.295}$	1.48	0.99	8.80	20	$R(Z, N_w) = 2.37 \times 10^{-3} Z^{0.654} N_w^{0.301}$	5.04	0.90	11.01

were computed at 20°C assuming a 10° width of the canting angle distribution (with a mean of 0°) and using the axis ratio relation specified by Brandes et al. (2002). Full details of the disdrometer dataset can be found in Schuur et al. (2001). These derived retrieval equations were found by performing weighted least squares regressions on the median of each variable within bins of $\log_{10}(R)$ and $\log_{10}(\mathrm{LWC})$ ranging from −1.2 to 2.0 and −2.2 to 1.0, respectively, in intervals of 0.1. Each bin was weighted by the center R or LWC within the bin multiplied by the number of points within that bin. The goal of deriving retrieval equations for R and LWC using the disdrometer data was to investigate the inherent usefulness of various polarimetric variables for rain retrievals, as each derived retrieval equation was found using the same method and dataset. A summary of all of these derived retrieval equations, along with their root-mean-square errors (RMSEs), are shown in Table 1.

Figure 1 is a Taylor diagram[1] (Taylor 2001) examining the utility of these derived retrieval equations for both R and LWC at S and C band. For both LWC and R at both wavelengths, retrievals using only Z perform the worst, with the largest RMSE, standard deviation, and lowest correlation with the disdrometer dataset. At S band, the $\mathrm{LWC}(Z, N_w)$ and $R(Z, N_w)$ retrievals show the best performance. The retrievals of $\mathrm{LWC}(Z, N_w)$ are also good at C band, while the error for $R(Z, N_w)$ at C band is a bit larger owing to resonance scattering complicating the Z–R relationship for larger raindrops.

In practice, however, the use of N_w may not be ideal. Estimates of N_w can be obtained from dual-pol data using the so-called "$Z - Z_{DR}$" method (Illingworth and Thompson 2005; Tabary et al. 2011), and estimates of median volume diameter D_0, which is quite close to D_m, can be found via Z_{DR} (e.g., Gorgucci et al. 2002; Cao et al. 2008), which can then be used to retrieve the LWC. However, accurate estimation of N_w requires high-quality, well-calibrated radar measurements of the intrinsic Z and Z_{DR}, which can become difficult at shorter wavelengths owing to attenuation. Additionally, to achieve estimates of Z and Z_{DR} with sufficient accuracy, the $Z - Z_{DR}$ method requires the use of multiple consecutive gates, resulting in a lower spatial resolution for N_w. Owing to potential difficulties in using N_w, alternative relations should also be considered. Second to $\mathrm{LWC}(Z, N_w)$, $\mathrm{LWC}(A_H)$ exhibits the smallest RMSE at S band, while $\mathrm{LWC}(K_{DP})$ exhibits the smallest RMSE at C band (although it also suffers from inferior resolution compared to the other polarimetric retrieval methods). For R retrievals, $R(A_H)$ retrievals feature the smallest RMSE at S band while at C band $R(K_{DP})$ has the smallest RMSE. For both LWC and R at both wavelengths, retrievals incorporating Z_{DR} improve upon those using Z alone but perform less well relative to the other polarimetric retrievals presented. The performance for $\mathrm{LWC}(Z, Z_{DR})$ and $R(Z, Z_{DR})$ retrievals will likely be even poorer in areas dominated by rain derived from melting hail and graupel, which tends to feature large drops with large Z_{DR} that falls even farther outside

[1] Taylor diagrams are useful for assessing overall performance of models compared to a reference dataset (in this case, disdrometer observations). The thick solid black line represents the standard deviation of the observations (σ_{obs}), with $0.5\sigma_{obs}$ and $1.5\sigma_{obs}$ denoted in dashed lines. Pearson correlation coefficient is shown as a function of angle α. RMSE values are shown in concentric thin gray rings centered at the observation point at the bottom of the plot (black dot), which corresponds to an RMSE of 0.0, a correlation of 1.0, and the standard deviation of the dataset. For example, LWC (A_H) at S band has a correlation coefficient of 0.96, a σ of 0.43, and an RMSE of 0.13 g m^{-3}, and is seen with a red star above and slightly to the right of the observation point.

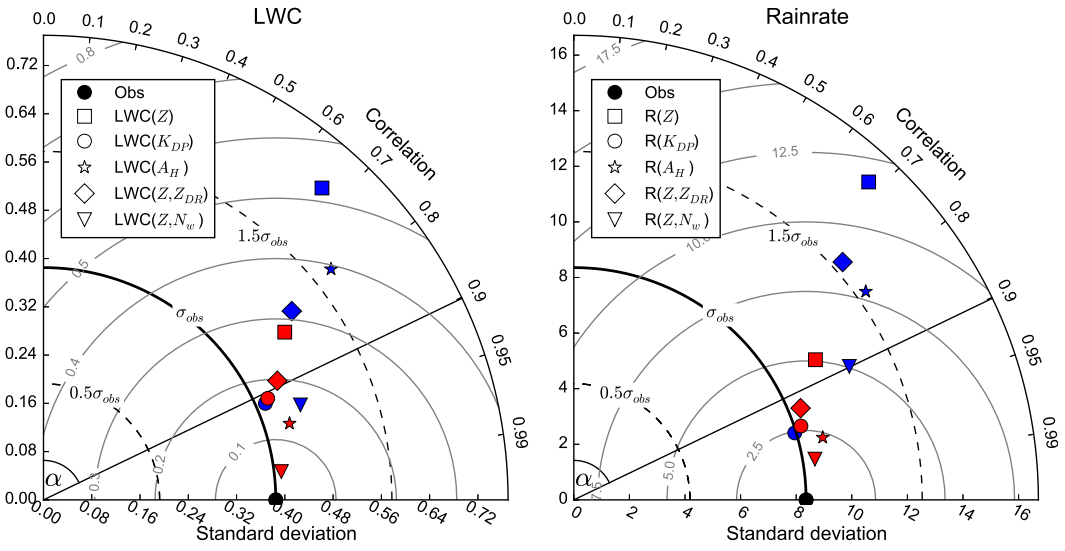

FIG. 1. Taylor diagram comparing the performance of retrievals at S band (red) and C band (blue) for (left) LWC ($g\,m^{-3}$) and (right) R ($mm\,h^{-1}$), corresponding to Eqs. (1)–(10) and (11)–(20) in Table 1, respectively. The black circle represents the characteristics of the observed disdrometer dataset. A line corresponding to a correlation of 0.9 is shown for improved readability.

of the typical $Z - Z_{DR}$ parameter space. Overall, with the exception of K_{DP}, all retrievals perform worse at C band than S band and for increasing RMSE exhibit higher standard deviations and lower correlations.

The above relations have been derived for the case of pure rain. In the case of a mixture of rain and hail, different relations must be used as both LWC and IWC must be estimated separately. To investigate this, spectral bin models were used that explicitly treat LWC and IWC separately. Additionally, such models allow the explicit estimation of N_w, providing guidance regarding the potential errors introduced by using the legacy LWC(Z) and $R(Z)$ relations. These models are described in the next section.

4. Description of spectral bin models used

Two spectral bin models were used to investigate the polarimetric characteristics of rain and hail as they relate to the legacy retrieval equations: a one-dimensional melting hail model (hereafter 1D-M) and the Hebrew University Cloud Model (HUCM). Unlike bulk microphysical parameterizations, in which some characteristics of the hydrometeor size distributions are prescribed a priori and the size distributions are restricted to a certain form [often an inverse exponential distribution, as in Eq. (12), or more generally a gamma distribution] and evolve as a whole, models with spectral bin microphysics divide the hydrometeor size distributions into different size bins that are treated independently, allowing for the better representation of processes that depend on differences in particle behavior along the size spectrum (e.g., aggregation) and therefore a more natural evolution of the size distribution than is allowed in bulk parameterizations. Owing to the prohibitive computational expense required for spectral bin microphysics, they have been limited to research applications while bulk microphysics have seen widespread operational use as a result of their ease of implementation and lower computational expense. Both spectral bin models used in this study feature a coupled polarimetric operator (Ryzhkov et al. 2011) to allow for the calculation of polarimetric radar variables. This operator treats particles as two-layer spheroids using the T-matrix formulation put forth by Bringi and Seliga (1977) and takes into account the size, shape, orientation, density, and mass liquid water fraction across the size spectrum of all hydrometeors using well-known parameterizations for quantities such as the dielectric constants, aspect ratios, and canting angles of the rain and ice distributions [for more details, see Ryzhkov et al. (2011)]. The two models used are intended to be complementary; the HUCM can explicitly calculate the development of hydrometeor PSDs in a natural manner but is contingent upon the specific initial environmental conditions, while the 1D-M must have hydrometeor size distributions prescribed but can model distributions whose parameters encompass the entire range of possible values observed in nature.

a. *One-dimensional melting hail model*

The 1D-M is a one-dimensional Lagrangian model that contains prescribed hail and graupel size distributions at the top of the model domain, coincident with the

0°C level, and follows them as they fall and melt. Melting, shedding of meltwater, differential sedimentation, and drop breakup are included in the model, but processes involving interactions between hailstones (e.g., collisions) or size bins are not included. Mass water fraction is allowed to vary across the size distribution and meltwater and ice cores are treated separately, with the mass water fraction counted as LWC and the remaining ice core counted as IWC. Polarimetric radar calculations were performed for both S band (λ = 11.0 cm) and C band (λ = 5.45 cm). The top of the model domain was set at 4 km and the relative humidity was 100% with a constant lapse rate of 6.5°C km^{-1}. All ice was assumed to be solid (ρ = 917 kg m^{-3}). Meltwater is allowed to accumulate on the surface of ice particles and begins to be shed once a critical threshold was reached. For more about the 1D-M see Ryzhkov et al. (2013a).

Based on previous findings of biexponential distributions within hailstorms (Smith et al. 1976), initial ice distributions were given by

$$N(D) = N_{0g}\exp(-\Lambda_g D) + N_{0h}\exp(-\Lambda_h D), \quad (23)$$

where N_{0g} = 8000 m^{-3} mm^{-1} and Λ_g = 1.6 mm^{-1} for all distributions. This graupel distribution was chosen to replicate a Marshall and Palmer (1948) raindrop distribution at the surface. Three size categories for the hail portion of the distributions were used: small ($10 < D_{max} \leq 25$ mm), large ($30 < D_{max} \leq 50$ mm), and giant ($55 < D_{max} \leq 75$ mm), with D_{max} varying in 5-mm increments. The slope parameter Λ_h varied in increments of 0.05 mm^{-1} such that the product $D_{max}\Lambda_h$ fell between approximately 5 and 11, following the findings of Ulbrich and Atlas (1982) and Cheng et al. (1985). The intercept parameter was computed according to $N_{0h} = A\Lambda_h^{4.11}$ following Cheng et al. (1985) and Federer and Waldvogel (1975) with A varying from 50 to 800 in increments of 50. Once the parameters of the graupel and hail distributions were specified, they were combined and treated as one encompassing ice distribution. A total of 1952 unique ice distributions were modeled. The parameters of these distributions are summarized in Table 2.

TABLE 2. Summary of the range of parameters used in determining the modeled hail distributions in the 1D-M.

Size	Λ_h	$\Delta\Lambda_h$	D_{max}	ΔD_{max}	A	ΔA
	(mm^{-1})	(mm^{-1})	(mm)	(mm)	—	—
Small	0.25–1.10	0.05	10–25	5	50–800	50
Large	0.10–0.30	0.05	30–50	5	50–800	50
Giant	0.05–0.25	0.05	55–75	5	50–800	50

b. Hebrew University Cloud Model

The HUCM is a state-of-the-art two-dimensional nonhydrostatic Eulerian spectral bin model (Khain et al. 2004, 2011; Ilotoviz et al. 2016). It contains 43 mass doubling bins for a wide array of hydrometeor classes, including a newly introduced "freezing drops" category, and includes both dry and wet hail growth with liquid water permitted above and below the 0°C level (Phillips et al. 2014, 2015). Hail and graupel are considered to be separate, distinct classes. All hydrometeor distributions evolve organically and do not need to be prescribed, with all essential microphysical processes included. The simulated storm was a hailstorm that struck Villingen-Schwenningen, Germany, on 28 June 2006 and caused significant damage (Noppel et al. 2010). The computational area was 120 km × 19 km with a grid spacing of Δx = 300 m and Δz = 100 m. Following Khain et al. (2011), the initial cloud condensation nuclei (CCN) concentration was set to 3000 cm^{-3} in the lowest 2 km and decreased exponentially with height above that, representing polluted conditions. Radar variables were computed every 1 min at S band. For more details about this storm and its modeling, see Noppel et al. (2010) and Khain et al. (2011).

5. Evolution of rain retrieval biases

Figure 2 shows the predicted LWC and Z due to rain throughout the life cycle of the simulated storm from the HUCM with different shades of color for the quantity logN_w. It is immediately apparent that the relation between LWC and Z in rain is highly variable and changes significantly over time.

At t = 2460 s (Figs. 2a,e), raindrops have begun to form atop the burgeoning updraft [as discussed in Khain et al. (2013)], with LWC approaching 1 g m^{-3}. Rapid size sorting due to differential sedimentation occurs with this initial rain, with most of the updraft featuring DSDs skewed toward smaller drops with relatively low Z for the given LWC. This is seen prominently in the N_w field with very high values throughout the updraft indicative of a categorical underestimation of LWC by the legacy retrieval equation. This underestimation could negatively impact efforts to achieve accurate initial conditions and subsequently reduce spinup time in convection-resolving models.

A very sharp transition to low values of N_w is seen on the bottom fringe of the rain field, representing the size sorted large drops that have fallen out almost instantly upon formation. By t = 2880 s (Figs. 2b,f), rain DSDs have matured and are reasonably close to that predicted by the legacy retrieval equation [Eq. (16)], although distinct signatures for both the updraft (z = 5–8 km) and

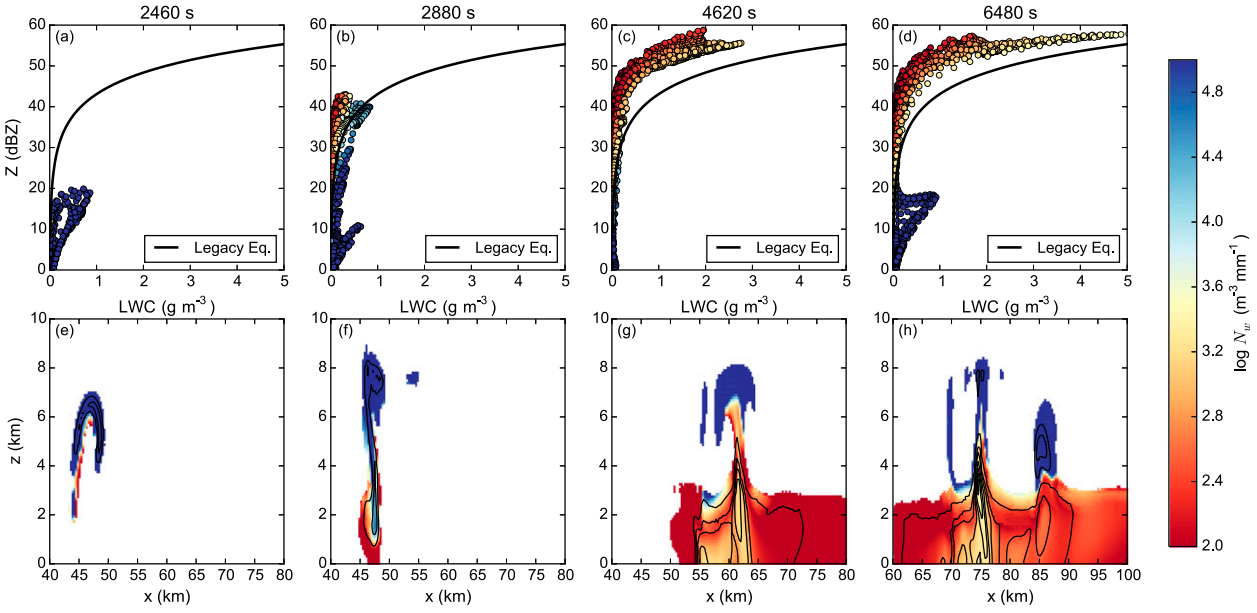

FIG. 2. Comparison of the legacy retrieval equation for rain [Eq. (16)] and LWC vs Z due to rain from the HUCM at (a),(e) $t = 2460$; (b),(f) $t = 2880$; (c),(g) $t = 4620$; and (d),(h) $t = 6480$ s. (top) The parameter space of the LWC vs Z relationship colored according to $\log_{10}N_w$ in comparison to the legacy retrieval equation. (bottom) The vertical cross section of $\log_{10}N_w$ (shown only for LWC $> 0.01\,\mathrm{g\,m^{-3}}$) at each time and LWC contoured at 0.1, 0.5, 1.0, 2.0, 3.0, and $4.0\,\mathrm{g\,m^{-3}}$.

size sorted drops ($z = 0$–2 km) still exist, resulting in a range of over 40 dBZ for LWCs under $1\,\mathrm{g\,m^{-3}}$.

Nearly 30 min later at $t = 4620$ s (Figs. 2c,g), the LWC–Z relationship has changed significantly, with the majority of rain found below the melting level and dominated by the melting of hail and graupel. Relatively low values of N_w are present in the entire region indicative of large drops and a categorical overestimation of LWC from the legacy retrieval equation by up to 500%. This is in agreement with previous studies (e.g., Ryzhkov et al. 2009) that found that melting graupel and hail can be associated with high Z_{DR} values. The predominance of rain generated from ice microphysical processes persists throughout the storm's life cycle once it has matured. The microphysical characteristics of the updraft have changed as well. By this time, a well-formed Z_{DR} column (e.g., Illingworth et al. 1987; Kumjian et al. 2014) is seen within the updraft as large raindrops are recycled into the updraft and undergo time-dependent freezing. In this region, the LWC–Z relationship is similar to that beneath the melting level. Outside of and above the Z_{DR} column, where raindrops have frozen and converted to hail or the freezing drops category, N_w rises sharply as the DSDs are once again skewed toward smaller drops. Finally, at $t = 6480$ s (Figs. 2d,h), a new updraft centered around $x = 86$ km and $z = 5$ km begins to develop, with high values and a very sharp gradient of N_w and an LWC–Z relationship similar to that seen at $t = 2460$ s. This occurs alongside the former updraft with a Z_{DR} column and widespread rain generated from ice, highlighting the spatial variability in the LWC–Z relationship that may exist at any given time in addition to the temporal variability.

It is clear that the variability in space and time of the LWC–Z relationship must be taken into account to achieve accurate retrievals. In all of these cases, the stratification of the LWC–Z relationship with respect to N_w is obvious, with N_w providing a clear indication of the bias of the legacy retrieval equation regardless of area or stage of development.

6. Retrievals in rain and hail mixtures

a. *Estimation of LWC*

In practice, it is not known a priori what the relative contributions of rain and hail are to the measured radar variables, where each measurement is a function of all hydrometeors contained in the volume. However, effective use of radar data for retrievals necessitates the separate estimation of LWC and IWC within the volume. The difficulties in accurately retrieving LWC using Z are exacerbated if hail is contained in the volume. Any information about LWC from Z is completely lost if even a small amount of hail is contained in the volume as hail can completely dominate the returned Z and result in a severe overestimation of LWC. Unfortunately, the calculation of A_H is corrupted in the presence of hail, so other methods must be sought.

The use of K_{DP} for retrieving R was suggested decades ago (e.g., Seliga and Bringi 1978; Doviak and Zrnić 1993; Ryzhkov and Zrnić 1995; Zrnić and Ryzhkov 1996) in order to improve quantitative precipitation estimation by lessening biases introduced by Z contaminated by hail (e.g., Aydin et al. 1995) and reducing sensitivity to rain drop size distribution variability. The premise of using K_{DP} in rain–hail mixtures is based on the assumption that it is immune to hail due to random tumbling that results in isotropic scattering. This assumption requires better justification for wet, melting hail that may stabilize and reduce the randomness of the tumbling.

Vertical profiles of IWC, LWC, and K_{DP} for each hail size category at both S and C band from the 1D-M are shown in Fig. 3. Within the 1D-M, there are three sources of hydrometeor mass: solid ice cores, the meltwater that collects on the surface of each ice core, and shed drops. Because modelers are generally concerned with the bulk values of LWC and IWC within a volume for retrievals, LWC was taken to be the sum of the surface meltwater and shedwater, while the ice cores were considered the IWC. While neither shedding nor breakup is a source (or sink) of LWC, both can affect the resultant polarimetric variables by modifying the rain DSD. In general, K_{DP} is positively correlated with the total LWC. For all of the modeled distributions, the large majority of graupel melts in the first 1.0–1.5 km below the melting level and contributes almost all of the LWC and K_{DP} in the first kilometer below the melting level, particularly for the distributions with larger hail (Figs. 3b,c,e,f). For small hail, the smaller hailstones also completely melt, resulting in a preponderance of large raindrops (see Fig. 5 in Ryzhkov et al. 2013a). This causes a slight enhancement of K_{DP} at S band (Fig. 3a) but a much larger enhancement at C band (Fig. 3d), where median K_{DP} values are $5.5^\circ\,km^{-1}$ and reach as high as $9.1^\circ\,km^{-1}$ as resonance effects become pronounced. Another slight enhancement can be seen between 2 and 3 km for large and giant hail at S band compared to C band (Figs. 3b,c). Shedding has not yet begun at these heights, so the increasing values of K_{DP} are due to meltwater on the surface of hailstones. This enhancement is notable at S band but almost nonexistent at C band (Figs. 3e,f), as also found for $R(K_{DP})$ retrievals in Ryzhkov et al. (2013b). These results are somewhat in contrast to the ideas discussed in Hubbert et al. (1998), who assumed that observed areas of enhanced K_{DP} aloft necessitates the presence of shed drops and are more in line with the results of Loney et al. (2002), whose in situ data supported a notable K_{DP} contribution from wet particles. With the exception of the effect of resonance scattering at C band for small hail, these deviations in the LWC–K_{DP} relation are relatively minor and K_{DP}, being quite constrained and immune to contributions from IWC, represents the potential for a marked improvement for retrieving LWC (performed in the following section) over the use of LWC(Z) in rain–hail mixtures.

b. Estimation of IWC

The estimation of IWC within a mixture also presents difficulties. One method to separate the contributions from rain and hail is to assume the hail is approximately isotropic (and therefore contributes negligibly to K_{DP}), estimate Z due to rain, Z_{LWC}, from K_{DP}, and then estimate IWC via the remaining Z which is assumed to be due to hail, Z_{IWC}, according to

$$Z_{IWC} = Z - Z_{LWC}, \tag{24}$$

where Z, Z_{IWC}, and Z_{LWC} are in linear units of $mm^6\,m^{-3}$ (Balakrishnan and Zrnić 1990; Doviak and Zrnić 1993). The Z_{LWC} –K_{DP} relations were derived from the disdrometer data following a procedure analogous to that described in section 3 and are as follows:

$$Z_{LWC} = 8.406 \times 10^4 (K_{DP})^{1.168}, \quad (\lambda = 11.0\,cm), \tag{25}$$

$$Z_{LWC} = 2.790 \times 10^4 (K_{DP})^{1.097}, \quad (\lambda = 5.33\,cm). \tag{26}$$

These relations are in good agreement with relations that can be derived from parameters reported in Doviak and Zrnić (1993) and Ryzhkov et al. (2013b) that implicitly assumed the standard Z_{LWC}– R relation $Z_{LWC} = 200R^{1.6}$ (Marshall and Palmer 1948), although our exponents are a bit lower. Both the Doviak and Zrnić (1993) and Ryzhkov et al. (2013b) sets of relations were also tested using the following procedure and achieved very similar results to Eqs. (25) and (26) (not shown).

Figure 4 shows median values from this method—calculating Z_{LWC} from K_{DP} using Eqs. (25) and (26), finding Z_{IWC} from Eq. (24), and retrieving IWC from Z_{IWC} using Eq. (21)—applied at both S band (Figs. 4a–e) and C band (Figs. 4f–j) for all size distributions from the 1D-M. Despite the good correlation between LWC and K_{DP}, there is no apparent functional relation between the retrieved Z_{IWC} and the actual IWC (Figs. 4e,j, in black). Consequently, the retrieved IWC using the legacy retrieval equation for hail (Figs. 4e,j, in color) exhibits very large errors (RMSEs of $2.93\,g\,m^{-3}$ at S band and $1.64\,g\,m^{-3}$ at C band) with almost no skill (Pearson correlations of −0.27 and −0.02 at S and C band, respectively). Sources of error in this technique could include the assumption that K_{DP} has only a negligible contribution from hail, the Z_{LWC}– K_{DP} relation, and the Z_{IWC}–IWC relation. The relationship between

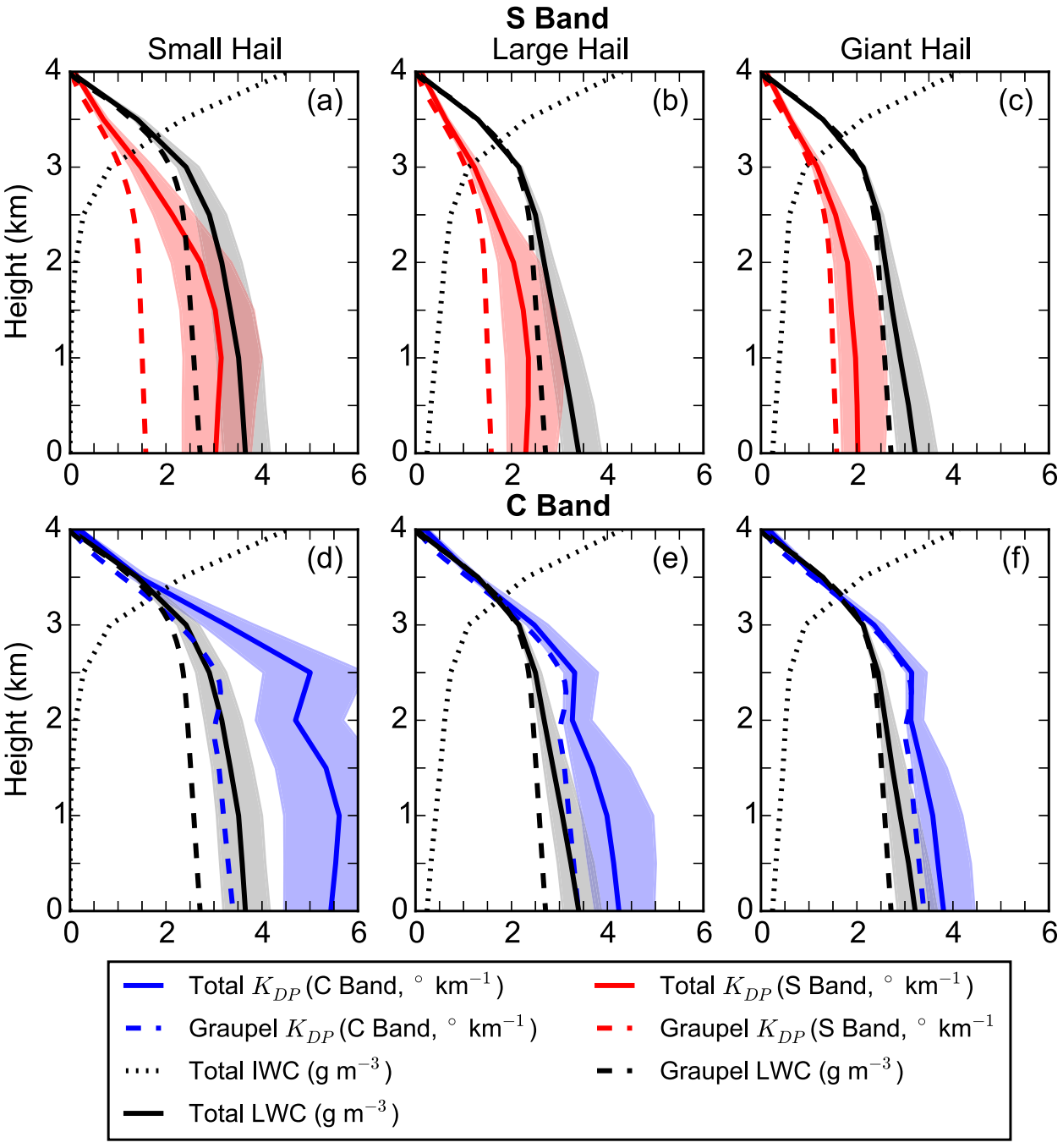

FIG. 3. Vertical profiles of median IWC (g m^{-3}, dotted black line), LWC (g m^{-3}, solid black line), and K_{DP} (° km^{-1}) at (a)–(c) S-band (solid red line) and (d)–(f) C-band (solid blue line) for (left to right) small, large, and giant hail from the 1D-M. The LWC and K_{DP} due to graupel alone at each wavelength are also shown in dashed black and red–blue lines, respectively. The shaded regions for total LWC and total K_{DP} depict the interquartile range of the distributions.

LWC and K_{DP} is in general quite immune to hail and robust (see previous section) although not perfect. Beyond the possible aforementioned slight impacts of accumulated meltwater at larger hail sizes at S band and possibly resonant effects from the melting of small hail at C band, the small but nonzero K_{DP} at 4 km above ground level ($\approx$0.08° km^{-1}) where only ice exists results in an estimated Z_{LWC} of approximately 35 dBZ. This is quite small in relation to the total Z, however, and should not introduce significant error into the retrieved

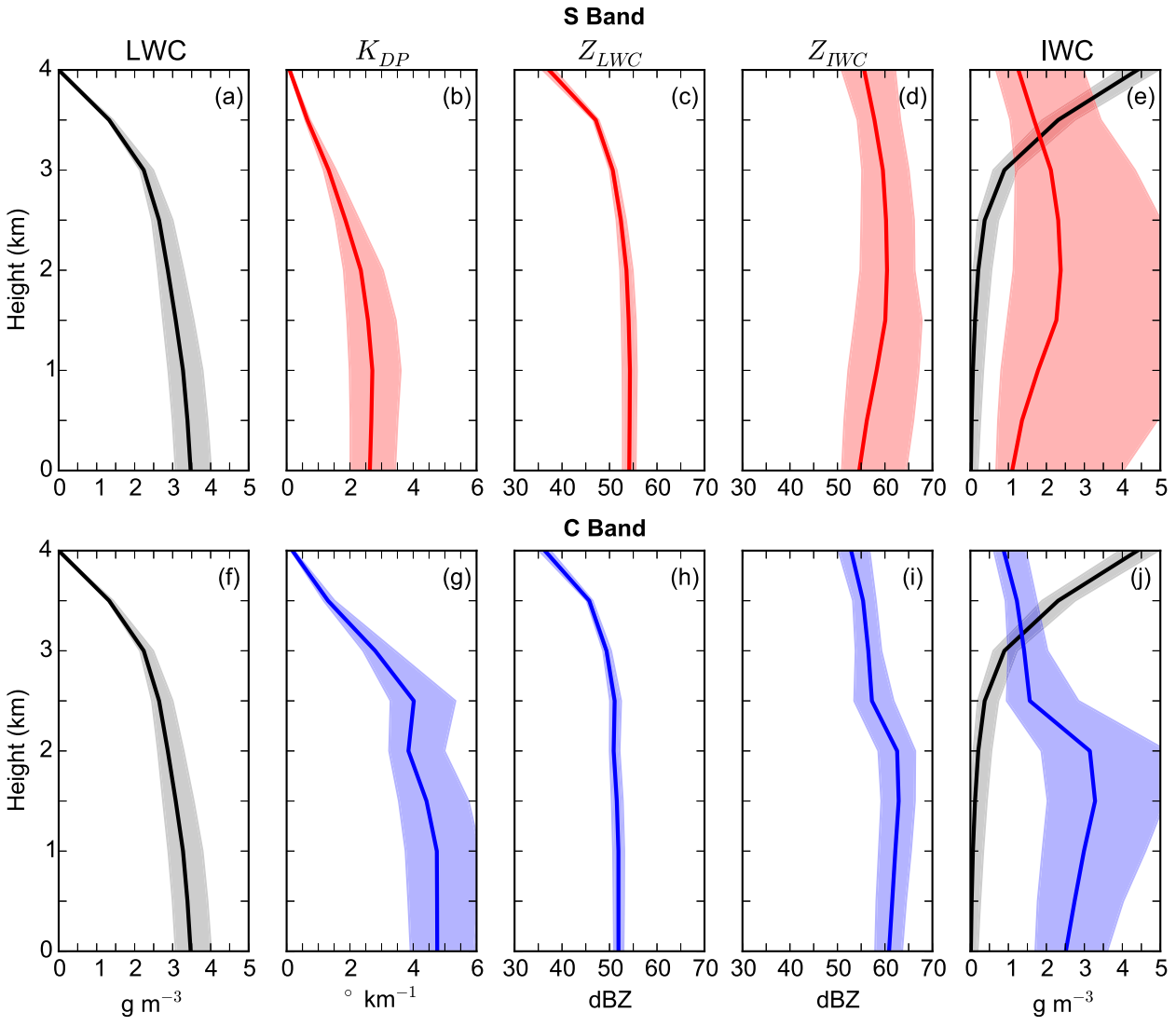

FIG. 4. Vertical profiles of median (a),(f) LWC (g m^{-3}), (b),(g) K_{DP} (° km^{-1}), (c),(h) retrieved Z_{LWC} (dBZ) using Eqs. (25) and (26), (d), (i) retrieved Z_{IWC} (dBZ) using Eq. (24), and (e),(j) IWC (black) and retrieved IWC (color) (g m^{-3}) using Eq. (21) from the 1D-M. The (top) S-band and (bottom) C-band calculations are shown in red and blue, respectively. The shaded regions depict the interquartile range of the distributions.

Z_{IWC}. The Z_{LWC}–K_{DP} relations, Eqs. (25) and (26), are robust and quite constrained, with RMSEs of 1.34 and 1.09 dBZ at S band and C band, respectively, for all values of Z. This RMSE increases to 3.07 dBZ at C band for Z_{LWC} greater than 40 dBZ due to the aforementioned resonance effects though the relationship is still a strong one. Since the contributions to Z are due to only rain and melting hail and graupel, the estimates of Z_{IWC} seem plausible and the significant errors in retrieved IWC are indeed due to the use of the legacy retrieval equation for hail.

This conclusion was examined in further detail in Fig. 5, in which the model IWC is plotted against the retrieved Z_{IWC} for all of the distributions from the 1D-M and compared to the legacy hail retrieval relation. In addition to radar wavelength and maximum hail size within the volume (where resonance effects may begin to affect Z measurements at larger sizes, even at S band), the strongest dependency is seen with respect to height below the melting level. For a decrease in IWC of two orders of magnitude, Z_{IWC} can remain nearly constant (e.g., Z_{IWC} = 60 dBZ corresponding to 5.5 g m^{-3} of IWC near the melting level to nearly no IWC near the surface). At both wavelengths, the use of the legacy retrieval equation results in a consistent negative bias in and above the melting layer and a positive bias below

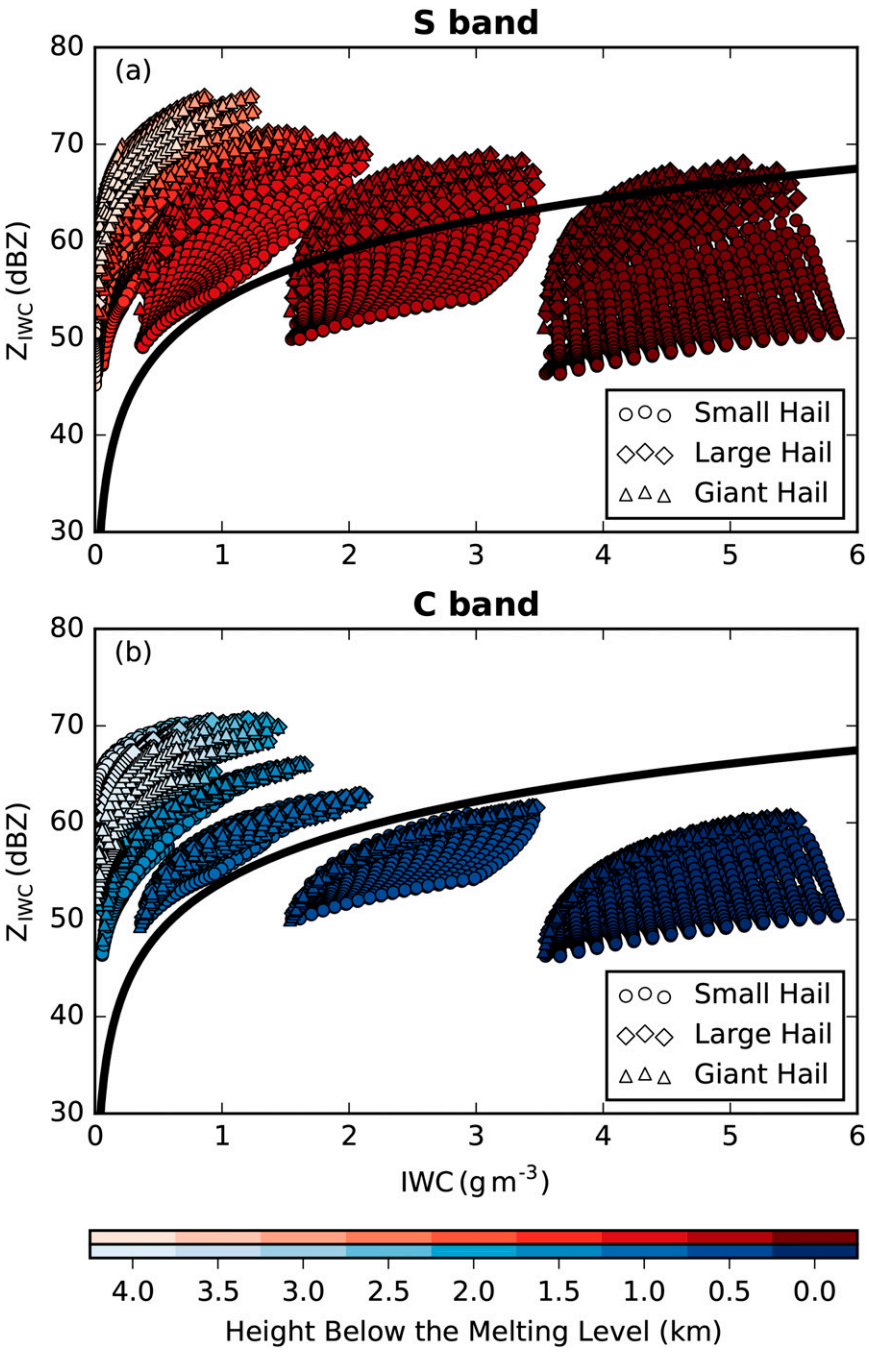

FIG. 5. IWC vs retrieved Z_{IWC} [via Eqs. (25) and (26)] for (a) S band (red) and (b) C band (blue), with separate markers for small, large, and giant hail. The legacy retrieval equation [Eq. (21)] is shown in black, and points are shaded according to their height below the melting level.

the melting layer, qualitatively similar to the findings for rain.

Figure 6 is a conceptual model showing the relative contributions to IWC and Z_{IWC} at both S and C band from mixed-phase particles of different sizes. Proportional to the third moment of the ice size distribution, the majority of the IWC is concentrated in the smaller sizes, and is particularly the case when significant amounts of graupel are present, as is necessarily the case for our results given the biexponential distributions modeled using the 1D-M. In contrast, Z_{IWC} is approximately equal to the sixth moment of the distribution and

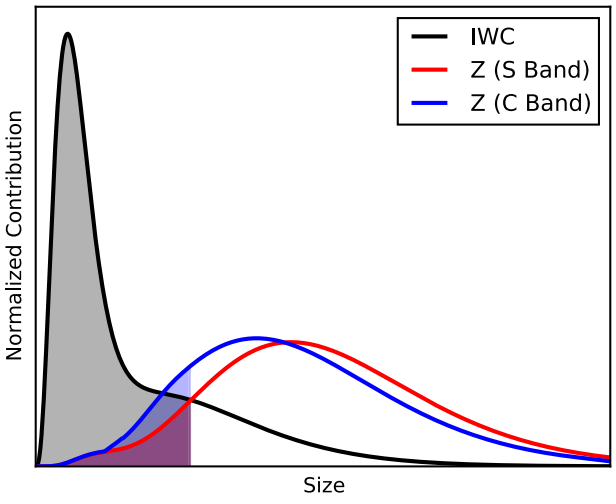

FIG. 6. Conceptual model of the normalized IWC (black) and Z (red, S band and blue, C band) as a function of size. The shading represents the contributions that may be removed due to total melting.

has a much broader maximum contribution at larger sizes. By the time the ice reaches the surface, all hail and graupel sizes below a certain size (represented by the shaded regions) have completely melted, representing a loss of the majority of the IWC. However, their contribution to Z_{IWC} was relatively low, and the larger hailstones that are the dominant contributors to Z_{IWC} do not contribute very much to the IWC. This also demonstrates the impact of the maximum hail size in the volume, which results in a decrease in Z_{IWC} while hardly affecting IWC. Additionally, the contribution to Z_{IWC} at C band is higher than at S band for small hail sizes and smaller than at S band for large hail sizes due to resonance effects playing a role at smaller hail sizes at C band (see Fig. 10 in Ryzhkov et al. 2013a). All of these factors result in a very indirect relationship between IWC and Z_{IWC}.

Based on these results, it is clear that radar wavelength, maximum hail size, and particularly the height below the melting layer of the radar resolution volume in question must be taken into account in order to retrieve accurate estimates of IWC. To demonstrate how the IWC(Z) relation changes with wavelength, height, and maximum hail size, power-law regressions of the form $Z_{IWC} = a(\text{IWC})^b$ were found at 500-m intervals below the melting level from the 1D-M results and are shown in Fig. 7. Distance below the melting level plays the dominant role over radar wavelength and maximum hail size, with the largest changes occurring in the first 2.0 km below the melting level before leveling off and becoming quite steady. Note that these coefficients are only valid for the atmospheric conditions prescribed in the 1D-M, although it is reasonable to expect that similar conclusions would hold for most atmospheric profiles beneath the melting layer representative of environmental conditions conducive to convection and hail production. These results are reflected in the proposed hail size discrimination algorithm (HSDA; Ryzhkov et al. 2013b), which seeks to identify the maximum hail size within a radar resolution volume by using the polarimetric variables in an analogous manner to the operational HCA. In agreement with our results, the membership functions are constant below 3 km below the melting level. Knowledge of the maximum hail size in a volume, radar wavelength, and height with respect to the melting level could then be used to select a more appropriate retrieval relation for more accurate estimates of IWC.

To further strengthen the justification for the estimation of Z_{IWC} presented above, the relationship between IWC and Z_{IWC} partitioned by height from the HUCM is shown in Fig. 8. Model output was accumulated over a 30-min period starting from when hail first reached the surface in order to capture the variability of IWC(Z) relations throughout the developing and mature stages of the storm at each height interval. Here, as before, IWC represents hail and graupel together due to the often abrupt conversion between the two categories in some cases in the HUCM microphysics [due to graupel reaching a size or density threshold; see Ilotoviz et al. (2016) for more details] as well as the fact that many microphysics schemes do not explicitly treat graupel and hail separately. This sudden transition is easily seen in Fig. 9a at $z = 4$–6 km.

The results seen in Fig. 8, for which Z_{IWC} is calculated explicitly and rigorously for each hydrometeor class, agree quite well with the retrieved Z_{IWC} from the 1D-M in Fig. 5. The legacy IWC(Z) relationship generally performs poorly above $z = 4$ km, where graupel dominates from the riming of snowflakes aloft before quickly melting below the melting level or converting to hail (Fig. 9a). For a given value of Z, graupel exhibits a much higher IWC than is predicted by the legacy hail retrieval equation due primarily to its higher concentration than the N_{0h} assumed in the hail retrieval equation, as well as having a lower density. The use of the legacy retrieval equations for hail will thus result in a severe underestimation of IWC aloft of up to 3 g m^{-3} through a large depth of the storm (Fig. 9g). A separate graupel retrieval relation should instead be considered.

At and below the melting level, the same biases found from the 1D-M are seen from the HUCM data. The use of the wet hail retrieval equation [Eq. (22)] does a better job than the dry hail retrieval equation [Eq. (21)], although both relations fail to capture the full variability

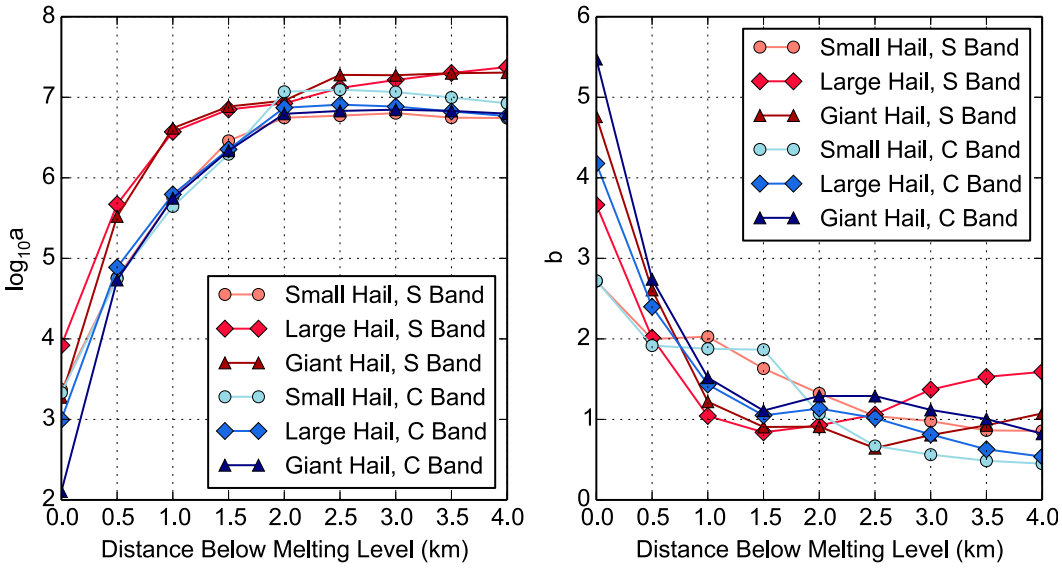

FIG. 7. Regression coefficients from the 1D-M of the form $Z_{IWC} = a(IWC)^b$ for (left) a and (right) b, where Z_{IWC} is in linear units of $mm^6\,m^{-3}$ and IWC is in $g\,m^{-3}$ for small, large, and giant hail at 500-m intervals below the melting level for S and C band.

of the IWC(Z) relation across all heights (Fig. 8) and would result in a positive bias in retrieved IWC below the melting level [e.g., Fig. 9g for Eq. (21)]. As the Z calculated for hail in the HUCM consists of both the ice core and surface meltwater, there is an increase in Z owing to the increase in the dielectric constant of hail as meltwater accumulates on the surface. However, the primary source of error in using a static hail retrieval equation comes from the precipitous loss of IWC as hail falls and melts. This is easily seen in Figs. 9b–e, where graupel and small hailstones melt very quickly into rain below the melting level while the largest hail, which dominates the Z_{IWC}, does not lose much mass. The hail mass distributions tend to become relatively stable about 2 km below the melting level (Figs. 9e,f) in good agreement with the 1D-M. Although this example is from an Eulerian frame of reference at a given time and therefore is not following the same volume of hail in a Lagrangian sense, the results are broadly consistent with the 1D-M as well as conceptual expectations of the impact of melting hail on Z.

7. Summary and conclusions

Radar data are the only source of hydrometeor information available for assimilation on the scale of convection-resolving models, which have seen a surge in development in the past two decades and will play an increasingly large role in the warning decision process of forecasters in the future. Both forward operators and retrieval equations can be used to accomplish this but often require many limiting assumptions.

The goal of this study was to investigate the utility of the most simplified versions of commonly used retrieval equations for LWC in pure rain and LWC and IWC within a rain–hail mixture and the consequences of making such assumptions. These simplified retrieval equations for rain, hail, and snow are derived in detail, and their assumptions and limitations are discussed.

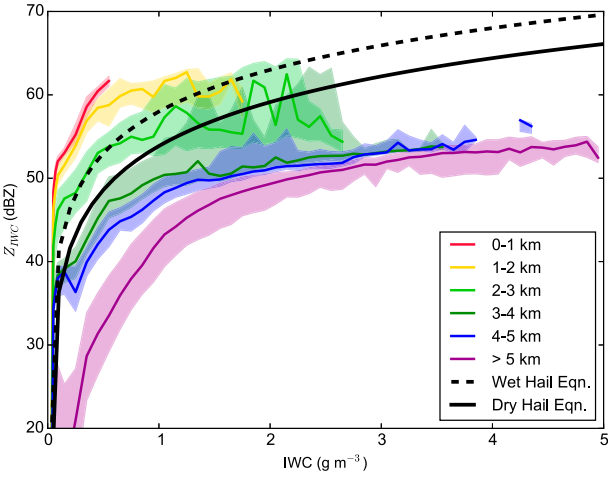

FIG. 8. Median Z_{IWC} for binned IWC (hail + graupel) from the HUCM partitioned by height (different colors) for bins with 10 or more points. IWC was binned at every $0.02\,g\,m^{-3}$ between 0.0 and $0.1\,g\,m^{-3}$ and at every $0.1\,g\,m^{-3}$ between 0.1 and $5.0\,g\,m^{-3}$. The shaded regions depict the interquartile range of the distributions. The legacy retrieval equations for dry [solid black; Eq. (21)] and wet hail [dashed black; Eq. (22)] are also shown. The melting level is at approximately $z = 3.5$ km.

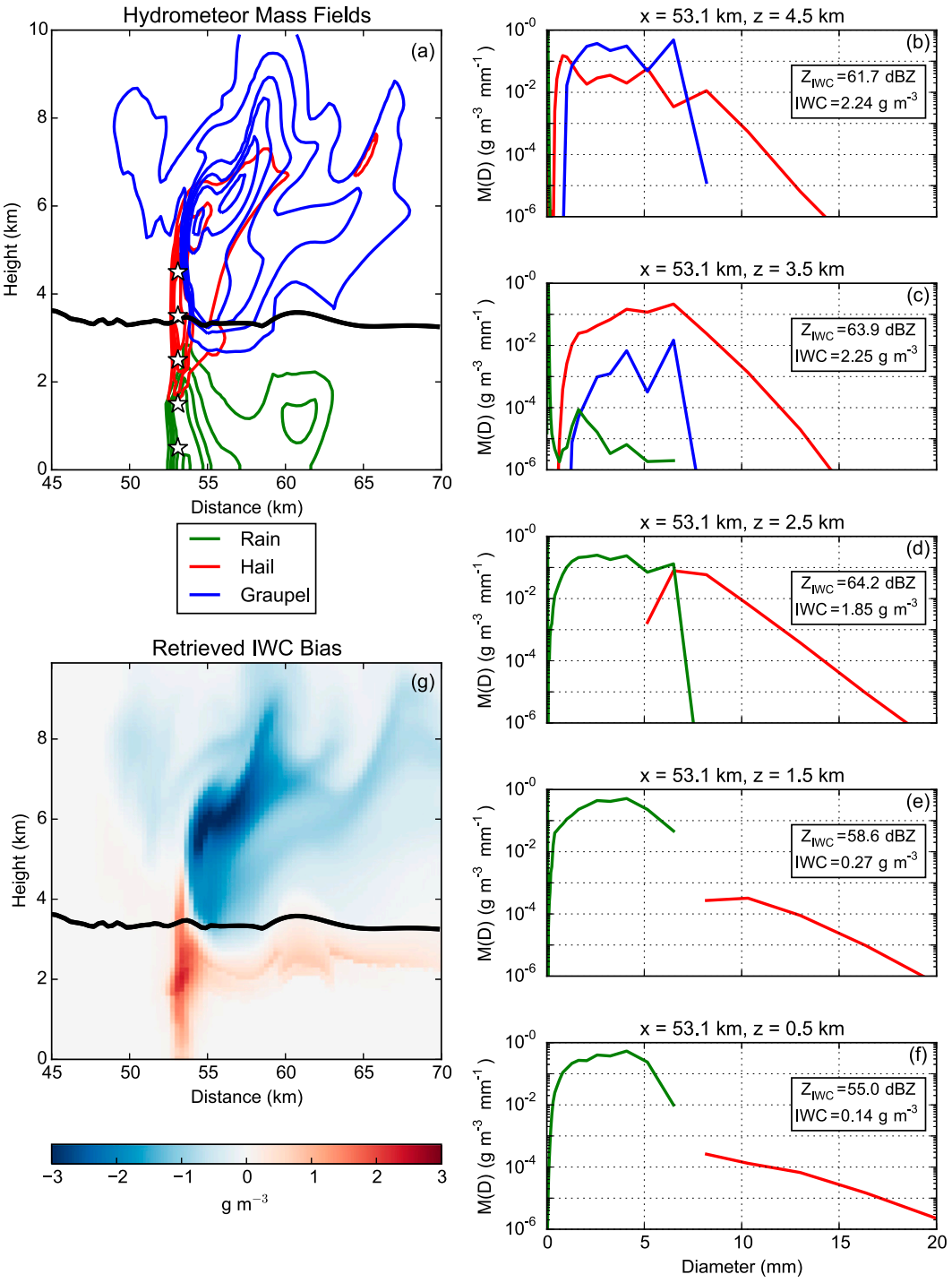

FIG. 9. HUCM output for $t = 4260$ s showing (a) contours of rain (green), hail (red), and graupel (blue) mass every 0.5 g m^{-3} beginning at 0.5 g m^{-3}. (b)–(f) Mass distributions of rain (green), hail (red), and graupel (blue) at 1-km intervals in the vertical (from 4.5 to 0.5 km, respectively) at $x = 53.1$ km and with the IWC and Z_{IWC} of the distributions shown. (g) The bias in retrieved IWC (g m^{-3}) when using the legacy retrieval equation [Eq. (21)]. The 0°C isotherm is shown in black in (a) and (g) and the stars in (a) denote the locations of the (b)–(f) sampled mass distributions.

Two spectral bin models are used in the study: a one-dimensional melting hail model, and the two-dimensional Hebrew University Cloud Model. The melting hail model is used to simulate the polarimetric radar characteristics of 1952 different melting hail size distributions for both S and C band. The Hebrew University Cloud Model is used to simulate a hailstorm from the start and to get a qualitative look at how the retrieval equations perform temporally and spatially. The general conclusions are as follows:

1) The relation between LWC and Z for rain varies significantly and is not constant in space or time, corroborating the results of many previous studies (e.g., Atlas and Chemla 1957; Battan 1973; Austin 1987). The use of the legacy retrieval equation for rain results in a systematic underestimation of LWC in developing updrafts and an overestimation of LWC in rain derived from melting hail and graupel, the dominant source of rain below the melting level in midlatitude convection. Size sorting processes will also limit the accuracy of the legacy retrieval equation. The use of N_w, which can be estimated from Z and Z_{DR}, offers clear insight into where and how severely the legacy retrieval equation will be biased.
2) In pure rain at both wavelengths, LWC(Z) exhibits the largest errors while incorporating N_w results in the best retrievals. Estimates of R are also superior when using N_w at S band. However, N_w suffers from reduced resolution when compared to other radar variables and may be more difficult to estimate accurately at C band due to possible attenuation affects. With that in mind, the best retrievals of R and LWC at S band are from A_H, which can be obtained with knowledge of the radar wavelength and a background temperature field from a model, while at C band the best retrievals of R and LWC are from K_{DP}. Both A_H and K_{DP} have the additional advantage over Z of being immune to radar miscalibration and partial beam blockage.
3) Within rain–hail mixtures, the LWC and IWC must be estimated separately. All information content about LWC in Z using the legacy retrieval equation is lost if even a small amount of hail is present in the volume. The calculation of A_H also fails in the presence of hail, so the use of K_{DP} to estimate the LWC in the presence of hail is recommended for both S and C band.
4) Once the LWC within a rain–hail mixture is known, the Z_{IWC} can be estimated. However, the legacy retrieval equation for hail may feature large errors, where neither the dry or wet forms of the legacy hail retrieval equation capture the full variability of the parameter space. A categorical underestimation of IWC exists above the melting level where lower-density graupel dominates the IWC, while a consistent overestimation of IWC below the melting level exists as Z is dominated by the largest hailstones while the bulk of the IWC comes from the smallest hailstones and graupel, which quickly melt below the melting level. The radar wavelength, maximum hail size, and especially the height below the melting level must be taken into account when attempting to retrieve the IWC.

Much remains to be done in the realm of polarimetric radar data assimilation, with the field still in its infancy and with the best way to assimilate this data remaining an active area of research. While more accurate estimates of LWC and IWC are desirable, they still represent only one moment of the particle size distributions and once assimilated will suffer from the same limitations exhibited when using single-moment microphysics. As such, future work will seek to investigate the impact of these improved hydrometeor retrievals on model forecasts. Beyond the rain–hail mixtures investigated here, more also needs to be done on the utility of retrievals for other hydrometeor types such as snow, ice crystals, etc. as well as their associated impacts.

A new paradigm in radar data assimilation is envisioned in which the benefits of polarimetry are fully capitalized on to improve storm-scale analyses and alleviate assumptions often used. For example, results from the polarimetric HCA could be used to aid in determining the dominant hydrometeor class in a volume and subsequently which retrieval equation to use instead of relying on empirical rules employing model background temperature. In addition to improving the quality of hydrometeor retrievals and helping to differentiate rain and hail [as extreme errors in LWC(Z) can result if a rain–hail mixture is assumed to be rain], dual-polarization data are also useful for detecting areas of size sorting through the ''big drops'' category in the operational HCA (Park et al. 2009). Additionally, polarimetric signatures often have connections to thermal and dynamical fields. For example, positive correlations have been shown to exist between Z_{DR} columns and updraft strength (Picca et al. 2010; Kumjian et al. 2014; Snyder et al. 2015) and between Z_{DR} arc characteristics and storm relative helicity within supercells (Kumjian and Ryzhkov 2009). Similarly, polarimetric signatures of hydrometeor phase changes (e.g., Kumjian et al. 2012, Kumjian and Ryzhkov 2010) should be investigated for their information content about latent heating to aid in reducing spinup time and obtaining more accurate storm-scale analyses.

Acknowledgments. This work originated in part from an M.S. thesis in the School of Meteorology at the University of Oklahoma. Funding was provided in part by NOAA/Office of Oceanic and Atmospheric Research under NOAA–University of Oklahoma Cooperative Agreement NA11OAR4320072, U.S. Department of Commerce. Partial support for this work comes from Grant ER65459 from the U.S. Department of Energy Atmospheric System Research program and from NSF Grant AGS-1341878. The authors thank Scott Ganson for his support of the T-matrix code used in the study. The authors also wish to thank Dr. Edward ''Ted'' Mansell for reviewing the manuscript and providing valuable suggestions, as well as the three anonymous reviewers whose constructive criticism helped improve the manuscript's clarity and focus.

REFERENCES

Aksoy, A., D. C. Dowell, and C. Snyder, 2009: A multicase comparative assessment of the ensemble Kalman filter for assimilation of radar observations. Part I: Storm-scale analyses. *Mon. Wea. Rev.*, **137**, 1805–1824, doi:10.1175/2008MWR2691.1.

Al-Sakka, H., A.-A. Boumahmoud, B. Fradon, S. J. Frasier, and P. Tabary, 2013: A new fuzzy logic hydrometeor classification scheme applied to the French X-, C-, and S-band polarimetric radars. *J. Appl. Meteor. Climatol.*, **52**, 2328–2344, doi:10.1175/JAMC-D-12-0236.1.

Atlas, D., and A. C. Chemla, 1957: Physical-synoptic variations of drop-size parameters. *Sixth Weather Radar Conf.*, Cambridge, MA, Amer. Meteor. Soc., 21–29.

——, and C. W. Ulbrich, 1977: Path- and area-integrated rainfall measurement by microwave attenuation in the 1–3 cm band. *J. Appl. Meteor.*, **16**, 1322–1331, doi:10.1175/1520-0450(1977)016<1322:PAAIRM>2.0.CO;2.

Austin, P. M., 1987: Relation between measured radar reflectivity and surface rainfall. *Mon. Wea. Rev.*, **115**, 1053–1070, doi:10.1175/1520-0493(1987)115<1053:RBMRRA>2.0.CO;2.

Aydin, K., V. N. Bringi, and L. Liu, 1995: Rain-rate estimation in the presence of hail using S-band specific differential phase and other radar parameters. *J. Appl. Meteor.*, **34**, 404–410, doi:10.1175/1520-0450-34.2.404.

Balakrishnan, N., and D. S. Zrnić, 1990: Estimation of rain and hail rates in mixed-phase precipitation. *J. Atmos. Sci.*, **47**, 565–583, doi:10.1175/1520-0469(1990)047<0565:EORAHR>2.0.CO;2.

Battan, L. J., 1973: *Radar Observations of the Atmosphere.* The University of Chicago Press, 324 pp.

Brandes, E. A., J. Vivekanandan, J. Tuttle, and C. Kessinger, 1995: A study of thunderstorm microphysics with multiparameter radar and aircraft observations. *Mon. Wea. Rev.*, **123**, 3129–3143, doi:10.1175/1520-0493(1995)123<3129:ASOTMW>2.0.CO;2.

——, G. Zhang, and J. Vivekanandan, 2002: Experiments in rainfall estimation with a polarimetric radar in a subtropical environment. *J. Appl. Meteor.*, **41**, 674–685, doi:10.1175/1520-0450(2002)041<0674:EIREWA>2.0.CO;2; Corrigendum. *J. Appl. Meteor.*, **44**, 186, doi:10.1175/1520-0450(2005)44<186:C>2.0.CO;2.

——, K. Ikeda, G. Zhang, M. Schönhuber, and R. M. Rasmussen, 2007: A statistical and physical description of hydrometeor distributions in Colorado snowstorms using a video disdrometer. *J. Appl. Meteor. Climatol.*, **46**, 634–650, doi:10.1175/JAM2489.1.

Brewster, K., 2002: Recent advances in the diabatic initialization of a non-hydrostatic numerical model. *15th Conf. on Numerical Weather Prediction/21st Conf. on Severe Local Storms*, San Antonio, TX, Amer. Meteor. Soc., J6.3. [Available online at https://ams.confex.com/ams/SLS_WAF_NWP/techprogram/paper_47414.htm.]

Bringi, V. N., and T. A. Seliga, 1977: Scattering from axisymmetric dielectrics or perfect conductors imbedded in an axisymmetric dielectric. *IEEE Trans. Antennas Propag.*, **25**, 575–580, doi:10.1109/TAP.1977.1141642.

——, and V. Chandrasekar, 2001: *Polarimetric Doppler Weather Radar: Principles and Applications.* Cambridge University Press, 636 pp.

——, ——, J. Hubbert, E. Gorgucci, W. L. Randeu, and M. Schoenhuber, 2003: Raindrop size distribution in different climatic regimes from disdrometer and dual-polarized radar analysis. *J. Atmos. Sci.*, **60**, 354–365, doi:10.1175/1520-0469(2003)060<0354:RSDIDC>2.0.CO;2.

Cao, Q., G. Zhang, E. Brandes, T. Schuur, A. Ryzhkov, and K. Ikeda, 2008: Analysis of video disdrometer and polarimetric radar data to characterize rain microphysics in Oklahoma. *J. Appl. Meteor. Climatol.*, **47**, 2238–2255, doi:10.1175/2008JAMC1732.1.

Chang, S.-F., Y.-C. Liou, J. Sun, and S.-L. Tai, 2016: The implementation of the ice phase microphysical process into a four-dimensional Variational Doppler Radar Analysis System (VDRAS) and its impact on parameter retrieval and quantitative precipitation nowcasting. *J. Atmos. Sci.*, **73**, 1015–1038, doi:10.1175/JAS-D-15-0184.1.

Cheng, L., M. English, and R. Wong, 1985: Hailstone size distributions and their relationship to storm thermodynamics. *J. Climate Appl. Meteor.*, **24**, 1059–1067, doi:10.1175/1520-0450(1985)024<1059:HSDATR>2.0.CO;2.

Cifelli, R., V. Chandrasekar, S. Lim, P. C. Kennedy, Y. Wang, and S. A. Rutledge, 2011: A new dual-polarization radar rainfall algorithm: Application in Colorado precipitation events. *J. Atmos. Oceanic Technol.*, **28**, 352–364, doi:10.1175/2010JTECHA1488.1.

Dawson, D. T., and M. Xue, 2006: Numerical forecasts of the 15–16 June 2002 Southern Plains mesoscale convective system: Impact of mesoscale data and cloud analysis. *Mon. Wea. Rev.*, **134**, 1607–1629, doi:10.1175/MWR3141.1.

——, L. J. Wicker, E. R. Mansell, and R. L. Tanamachi, 2012: Impact of the environmental low-level wind profile on ensemble forecasts of the 4 May 2007 Greensburg, Kansas, tornadic storm and associated mesocyclones. *Mon. Wea. Rev.*, **140**, 696–716, doi:10.1175/MWR-D-11-00008.1.

——, M. Xue, J. A. Milbrandt, and A. Shapiro, 2015: Sensitivity of real-data simulations of the 3 May 1999 Oklahoma City tornadic supercell and associated tornadoes to multimoment microphysics. Part I: Storm- and tornado-scale numerical forecasts. *Mon. Wea. Rev.*, **143**, 2241–2265, doi:10.1175/MWR-D-14-00279.1.

Doviak, R. J., and D. S. Zrnić, 1993: *Doppler Radar and Weather Observations.* Dover Publications, 562 pp.

Dowell, D. C., L. J. Wicker, and C. Snyder, 2011: Ensemble Kalman filter assimilation of radar observations of the 8 May 2003 Oklahoma City supercell: Influences of reflectivity observations on storm-scale analyses. *Mon. Wea. Rev.*, **139**, 272–294, doi:10.1175/2010MWR3438.1.

Droegemeier, K., 1990: Toward a science of storm-scale prediction. *16th Conf. on Severe Local Storms.*, Kananaskis Park, AB, Canada, Amer. Meteor. Soc., 256–262.

Evensen, G., 1994: Sequential data assimilation with a nonlinear quasi-geostrophic model using Monte Carlo methods to forecast error statistics. *J. Geophys. Res.*, **99**, 10 143–10 162, doi:10.1029/94JC00572.

Federer, B., and A. Waldvogel, 1975: Hail and raindrop size distributions from a Swiss multicell storm. *J. Appl. Meteor.*, **14**, 91–97, doi:10.1175/1520-0450(1975)014<0091:HARSDF>2.0.CO;2.

Gao, J., and D. J. Stensrud, 2012: Assimilation of reflectivity data in a convective-scale, cycled 3DVAR framework with hydrometeor classification. *J. Atmos. Sci.*, **69**, 1054–1065, doi:10.1175/JAS-D-11-0162.1.

——, M. Xue, K. Brewster, and K. K. Droegemeier, 2004: A three-dimensional variational data analysis method with recursive filter for Doppler radars. *J. Atmos. Oceanic Technol.*, **21**, 457–469, doi:10.1175/1520-0426(2004)021<0457:ATVDAM>2.0.CO;2.

Gorgucci, E., V. Chandrasekar, V. N. Bringi, and G. Scarchilli, 2002: Estimation of raindrop size distribution parameters from polarimetric radar measurements. *J. Atmos. Sci.*, **59**, 2373–2384, doi:10.1175/1520-0469(2002)059<2373:EORSDP>2.0.CO;2.

Gunn, K., and J. Marshall, 1958: The distribution with size of aggregate snowflakes. *J. Meteor.*, **15**, 452–461, doi:10.1175/1520-0469(1958)015<0452:TDWSOA>2.0.CO;2.

Hu, M., and M. Xue, 2007: Impact of configurations of rapid intermittent assimilation of WSR-88D radar data for the 8 May 2003 Oklahoma City tornadic thunderstorm case. *Mon. Wea. Rev.*, **135**, 507–525, doi:10.1175/MWR3313.1.

——, ——, and K. Brewster, 2006a: 3DVAR and cloud analysis with WSR-88D level-II data for the prediction of the Fort Worth, Texas, tornadic thunderstorms. Part I: Cloud analysis and its impact. *Mon. Wea. Rev.*, **134**, 675–698, doi:10.1175/MWR3092.1.

——, ——, J. Gao, and K. Brewster, 2006b: 3DVAR and cloud analysis with WSR-88D level-II data for the prediction of the Fort Worth, Texas, tornadic thunderstorms. Part II: Impact of radial velocity analysis via 3DVAR. *Mon. Wea. Rev.*, **134**, 699–721, doi:10.1175/MWR3093.1.

Hubbert, J., V. N. Bringi, L. D. Carley, and S. Bolen, 1998: CSU-CHILL polarimetric radar measurements from a severe hail storm in eastern Colorado. *J. Appl. Meteor.*, **37**, 749–775, doi:10.1175/1520-0450(1998)037<0749:CCPRMF>2.0.CO;2.

Illingworth, A. J., and R. J. Thompson, 2005: The estimation of moderate rain rates with operational polarisation radar. *32nd Int. Conf. on Radar Meteorology*, Albuquerque, NM, Amer. Meteor. Soc., P9R.1. [Available online at https://ams.confex.com/ams/pdfpapers/96204.pdf.]

——, J. W. F. Goddard, and S. M. Cherry, 1987: Polarization radar studies of precipitation development in convective storms. *Quart. J. Roy. Meteor. Soc.*, **113**, 469–489, doi:10.1002/qj.49711347604.

Ilotoviz, E., A. P. Khain, N. Benmoshe, V. T. J. Phillips, and A. V. Ryzhkov, 2016: Effect of aerosols on freezing drops, hail, and precipitation in a midlatitude storm. *J. Atmos. Sci.*, **73**, 109–144, doi:10.1175/JAS-D-14-0155.1.

Jung, Y., G. Zhang, and M. Xue, 2008: Assimilation of simulated polarimetric radar data for a convective storm using the ensemble Kalman filter. Part I: Observation operators for reflectivity and polarimetric variables. *Mon. Wea. Rev.*, **136**, 2228–2245, doi:10.1175/2007MWR2083.1.

——, M. Xue, and M. Tong, 2012: Ensemble Kalman filter analyses of the 29–30 May 2004 Oklahoma tornadic thunderstorm using one- and two-moment bulk microphysics schemes, with verification against polarimetric radar data. *Mon. Wea. Rev.*, **140**, 1457–1475, doi:10.1175/MWR-D-11-00032.1.

Kain, J. S., and Coauthors, 2010: Assessing advances in the assimilation of radar data and other mesoscale observations within a collaborative forecasting–research environment. *Wea. Forecasting*, **25**, 1510–1521, doi:10.1175/2010WAF2222405.1.

Kessler, E., Ed., 1969: *On the Distribution and Continuity of Water Substance in Atmospheric Circulations. Meteor. Monogr.*, No. 32, Amer. Meteor. Soc., 84 pp.

Khain, A., A. Pokrovsky, M. Pinsky, A. Seifert, and V. Phillips, 2004: Simulation of effects of atmospheric aerosols on deep turbulent convective clouds using a spectral microphysics mixed-phase cumulus cloud model. Part I: Model description and possible applications. *J. Atmos. Sci.*, **61**, 2963–2982, doi:10.1175/JAS-3350.1.

——, D. Rosenfeld, A. Pokrovsky, U. Blahak, and A. Ryzhkov, 2011: The role of CCN in precipitation and hail in a mid-latitude storm as seen in simulations using a spectral (bin) microphysics model in a 2D dynamic frame. *Atmos. Res.*, **99**, 129–146, doi:10.1016/j.atmosres.2010.09.015.

——, T. Prabha, N. Benmoshe, G. Pandithurai, and M. Ovchinnikov, 2013: The mechanism of first raindrops formation in deep convective clouds. *J. Geophys. Res. Atmos.*, **118**, 9123–9140, doi:10.1002/jgrd.50641.

Kumjian, M. R., 2013a: Principles and applications of dual-polarization weather radar. Part I: Description of the polarimetric radar variables. *J. Oper. Meteor.*, **1**, 226–242, doi:10.15191/nwajom.2013.0119.

——, 2013b: Principles and applications of dual-polarization weather radar. Part II: Warm- and cold-season applications. *J. Oper. Meteor.*, **1**, 243–264, doi:10.15191/nwajom.2013.0120.

——, 2013c: Principles and applications of dual-polarization weather radar. Part III: Artifacts. *J. Oper. Meteor.*, **1**, 265–274, doi:10.15191/nwajom.2013.0121.

——, and A. V. Ryzhkov, 2008: Polarimetric signatures in supercell thunderstorms. *J. Appl. Meteor. Climatol.*, **47**, 1940–1961, doi:10.1175/2007JAMC1874.1.

——, and ——, 2009: Storm-relative helicity revealed from polarimetric radar measurements. *J. Atmos. Sci.*, **66**, 667–685, doi:10.1175/2008JAS2815.1.

——, and ——, 2010: The impact of evaporation on polarimetric characteristics of rain: Theoretical model and practical implications. *J. Appl. Meteor. Climatol.*, **49**, 1247–1267, doi:10.1175/2010JAMC2243.1.

——, S. M. Ganson, and A. V. Ryzhkov, 2012: Freezing of raindrops in deep convective updrafts: A microphysical and polarimetric model. *J. Atmos. Sci.*, **69**, 3471–3490, doi:10.1175/JAS-D-12-067.1.

——, A. P. Khain, N. Benmoshe, E. Ilotoviz, A. V. Ryzhkov, and V. T. Phillips, 2014: The anatomy and physics of Z_{DR} columns: Investigating a polarimetric radar signature with a spectral bin microphysical model. *J. Appl. Meteor. Climatol.*, **53**, 1820–1843, doi:10.1175/JAMC-D-13-0354.1.

Li, X., and J. Mecikalski, 2010: Assimilation of the dual-polarization Doppler radar data for a convective storm with a warm-rain radar forward operator. *J. Geophys. Res.*, **115**, D16208, doi:10.1029/2009JD013666.

Lilly, D. K., 1990: Numerical prediction of thunderstorms—Has its time come? *Quart. J. Roy. Meteor. Soc.*, **116**, 779–798, doi:10.1002/qj.49711649402.

Lim, S., V. Chandrasekar, and V. N. Bringi, 2005: Hydrometeor classification system using dual-polarization radar

measurements: Model improvements and in situ verification. *IEEE Trans. Geosci. Remote Sens.*, **43**, 792–801, doi:10.1109/TGRS.2004.843077.

Liu, H., and V. Chandrasekar, 2000: Classification of hydrometeors based on polarimetric radar measurements: Development of fuzzy logic and neuro-fuzzy systems, and in situ verification. *J. Atmos. Oceanic Technol.*, **17**, 140–164, doi:10.1175/1520-0426(2000)017<0140:COHBOP>2.0.CO;2.

Loney, M. L., D. S. Zrnić, J. M. Straka, and A. V. Ryzhkov, 2002: Enhanced polarimetric radar signatures above the melting level in a supercell storm. *J. Appl. Meteor.*, **41**, 1179–1194, doi:10.1175/1520-0450(2002)041<1179:EPRSAT>2.0.CO;2.

Marshall, J. S., and W. M. K. Palmer, 1948: The distribution of raindrops with size. *J. Meteor.*, **5**, 165–166, doi:10.1175/1520-0469(1948)005<0165:TDORWS>2.0.CO;2.

Noppel, H., U. Blahak, A. Seifert, and K. D. Beheng, 2010: Simulations of a hailstorm and the impact of CCN using an advanced two-moment cloud microphysical scheme. *Atmos. Res.*, **96**, 286–301, doi:10.1016/j.atmosres.2009.09.008.

Pan, Y., M. Xue, and G. Ge, 2016: Incorporating diagnosed intercept parameters and the graupel category within the ARPS cloud analysis system for the initialization of double-moment microphysics: Testing with a squall line over south China. *Mon. Wea. Rev.*, **144**, 371–392, doi:10.1175/MWR-D-15-0008.1.

Park, H., A. V. Ryzhkov, D. S. Zrnić, and K.-E. Kim, 2009: The hydrometeor classification algorithm for the polarimetric WSR-88D: Description and application to an MCS. *Wea. Forecasting*, **24**, 730–748, doi:10.1175/2008WAF2222205.1.

Phillips, V. T. J., A. P. Khain, N. Benmoshe, A. V. Ryzhkov, and E. Ilotoviz, 2014: Theory of time-dependent freezing. Part I: Description of scheme for wet growth of hail. *J. Atmos. Sci.*, **71**, 4527–4557, doi:10.1175/JAS-D-13-0375.1.

——, ——, ——, ——, and ——, 2015: Theory of time-dependent freezing. Part II: Scheme for freezing raindrops and simulations by a cloud model with spectral bin microphysics. *J. Atmos. Sci.*, **72**, 262–286, doi:10.1175/JAS-D-13-0376.1.

Picca, J. C., M. Kumjian, and A. Ryzhkov, 2010: Z_{DR} columns as a predictive tool for hail growth and storm evolution. *25th Conf. on Severe Local Storms*, Denver, CO, Amer. Meteor. Soc., 11.3. [Available online at https://ams.confex.com/ams/25SLS/techprogram/paper_175750.htm.]

Ryzhkov, A. V., and D. S. Zrnić, 1995: Comparison of dual-polarization radar estimators of rain. *J. Atmos. Oceanic Technol.*, **12**, 249–256, doi:10.1175/1520-0426(1995)012<0249:CODPRE>2.0.CO;2.

——, S. E. Giangrande, and T. J. Schuur, 2005a: Rainfall estimation with a polarimetric prototype of WSR-88D. *J. Appl. Meteor.*, **44**, 502–515, doi:10.1175/JAM2213.1.

——, T. J. Schuur, D. W. Burgess, P. L. Heinselman, S. E. Giangrande, and D. S. Zrnić, 2005b: The Joint Polarization Experiment: Polarimetric rainfall measurements and hydrometeor classification. *Bull. Amer. Meteor. Soc.*, **86**, 809–824, doi:10.1175/BAMS-86-6-809.

——, S. Ganson, M. Pinsky, and A. Pokrovsky, 2009: Polarimetric characteristics of melting hail at S and C bands. *34th Conf. on Radar Meteorology*, Williamsburg, VA, Amer. Meteor. Soc., 4A.6. [Available online at http://ams.confex.com/ams/pdfpapers/155571.pdf.]

——, M. Pinsky, A. Pokrovsky, and A. Khain, 2011: Polarimetric radar observation operator for a cloud model with spectral microphysics. *J. Appl. Meteor. Climatol.*, **50**, 873–894, doi:10.1175/2010JAMC2363.1.

——, M. R. Kumjian, S. M. Ganson, and A. P. Khain, 2013a: Polarimetric radar characteristics of melting hail. Part I: Theoretical simulations using spectral microphysical modeling. *J. Appl. Meteor. Climatol.*, **52**, 2849–2870, doi:10.1175/JAMC-D-13-073.1.

——, ——, ——, and P. Zhang, 2013b: Polarimetric radar characteristics of melting hail. Part II: Practical implications. *J. Appl. Meteor. Climatol.*, **52**, 2871–2886, doi:10.1175/JAMC-D-13-074.1.

——, M. Diederich, P. Zhang, and C. Simmer, 2014: Potential utilization of specific attenuation for rainfall estimation, mitigation of partial beam blockage, and radar networking. *J. Atmos. Oceanic Technol.*, **31**, 599–619, doi:10.1175/JTECH-D-13-00038.1.

Schenkman, A. D., M. Xue, A. Shapiro, K. Brewster, and J. Gao, 2011a: The analysis and prediction of the 8–9 May 2007 Oklahoma tornadic mesoscale convective system by assimilation WSR-88D and CASA radar data using 3DVAR. *Mon. Wea. Rev.*, **139**, 224–246, doi:10.1175/2010MWR3336.1.

——, ——, ——, K. A. Brewster, and J. Gao, 2011b: Impact of CASA radar and Oklahoma mesonet data assimilation on the analysis and prediction of tornadic mesovortices in an MCS. *Mon. Wea. Rev.*, **139**, 3422–3445, doi:10.1175/MWR-D-10-05051.1.

Schuur, T. J., A. V. Ryzhkov, D. S. Zrnić, and M. Schönhuber, 2001: Drop size distributions measured by a 2D video disdrometer: Comparison with dual-polarization radar data. *J. Appl. Meteor.*, **40**, 1019–1034, doi:10.1175/1520-0450(2001)040<1019:DSDMBA>2.0.CO;2.

Seliga, T. A., and V. N. Bringi, 1976: Potential use of radar differential reflectivity measurements at orthogonal polarizations for measuring precipitation. *J. Appl. Meteor.*, **15**, 69–76, doi:10.1175/1520-0450(1976)015<0069:PUORDR>2.0.CO;2.

——, and ——, 1978: Differential reflectivity and differential phase shift: Applications in radar meteorology. *Radio Sci.*, **13**, 271–275, doi:10.1029/RS013i002p00271.

——, ——, and H. H. Al-Khatib, 1981: A preliminary study of comparative measurements of rainfall rate using the differential reflectivity radar technique and a raingage network. *J. Appl. Meteor.*, **20**, 1362–1368, doi:10.1175/1520-0450(1981)020<1362:APSOCM>2.0.CO;2.

Smith, P. L., 1984: Equivalent radar reflectivity factors for snow and ice particles. *J. Climate Appl. Meteor.*, **23**, 1258–1260, doi:10.1175/1520-0450(1984)023<1258:ERRFFS>2.0.CO;2.

——, C. G. Myers, and H. D. Orville, 1975: Radar reflectivity factor calculations in numerical cloud models using bulk parameterization of precipitation. *J. Appl. Meteor.*, **14**, 1156–1165, doi:10.1175/1520-0450(1975)014<1156:RRFCIN>2.0.CO;2.

——, D. J. Musil, S. F. Weber, J. F. Spahn, G. N. Johnson, and W. R. Sand, 1976: Raindrop and hailstone distributions inside hailstorms. *17th Int. Conf. on Cloud Physics*, Boulder, CO, Amer. Meteor. Soc., 252–257.

Snyder, J. C., H. B. Bluestein, G. Zhang, and S. J. Frasier, 2010: Attenuation correction and hydrometeor classification of high-resolution, X-band, dual-polarized mobile radar measurements in severe convective storms. *J. Atmos. Oceanic Technol.*, **27**, 1979–2001, doi:10.1175/2010JTECHA1356.1.

——, A. V. Ryzhkov, M. R. Kumjian, A. P. Khain, and J. Picca, 2015: A Z_{DR} column detection algorithm to examine convective storm updrafts. *Wea. Forecasting*, **30**, 1819–1844, doi:10.1175/WAF-D-15-0068.1.

Souto, M. J., C. F. Balseiro, V. Pérez-Muñuzuri, M. Xue, and K. Brewster, 2003: Impact of cloud analysis on numerical

weather prediction in the Galician region of Spain. *J. Appl. Meteor.*, **42**, 129–140, doi:10.1175/1520-0450(2003)042<0129:IOCAON>2.0.CO;2.

Stensrud, D. J., and J. Gao, 2010: Importance of horizontally inhomogeneous environmental initial conditions to ensemble storm-scale radar data assimilation and very short-range forecasts. *Mon. Wea. Rev.*, **138**, 1250–1272, doi:10.1175/2009MWR3027.1.

——, and Coauthors, 2009: Convective-scale Warn-on-Forecast system: A vision for 2020. *Bull. Amer. Meteor. Soc.*, **90**, 1487–1499, doi:10.1175/2009BAMS2795.1.

——, and Coauthors, 2013: Progress and challenges with Warn-on-Forecast. *Atmos. Res.*, **123**, 2–16, doi:10.1016/j.atmosres.2012.04.004.

Straka, J. M., D. S. Zrnić, and A. V. Ryzhkov, 2000: Bulk hydrometeor classification using polarimetric radar data: Synthesis of relations. *J. Appl. Meteor.*, **39**, 1341–1372, doi:10.1175/1520-0450(2000)039<1341:BHCAQU>2.0.CO;2.

Sun, J., 2005: Convective-scale assimilation of radar data: Progress and challenges. *Quart. J. Roy. Meteor. Soc.*, **131**, 3439–3463, doi:10.1256/qj.05.149.

——, and A. N. Crook, 1998: Dynamical and microphysical retrieval from Doppler radar observations using a cloud model and its adjoint. Part II: Retrieval experiments of an observed Florida convective storm. *J. Atmos. Sci.*, **55**, 835–852, doi:10.1175/1520-0469(1998)055<0835:DAMRFD>2.0.CO;2.

Tabary, P., A.-A. Boumahmoud, H. Andrieu, R. J. Thompson, A. J. Illingworth, E. Le Bouar, and J. Testud, 2011: Evaluation of two ''integrated'' polarimetric quantitative precipitation estimation (QPE) algorithms at C-band. *J. Hydrol.*, **405**, 248–260, doi:10.1016/j.jhydrol.2011.05.021.

Taylor, K. E., 2001: Summarizing multiple aspects of model performance in a single diagram. *J. Geophys. Res.*, **106**, 7183–7192, doi:10.1029/2000JD900719.

Testud, J., S. Oury, R. A. Black, P. Amayenc, and X. Dou, 2001: The concept of ''normalized'' distribution to describe raindrop spectra: A tool for cloud physics and cloud remote sensing. *J. Appl. Meteor.*, **40**, 1118–1140, doi:10.1175/1520-0450(2001)040<1118:TCONDT>2.0.CO;2.

Thompson, E., S. Rutledge, B. Dolan, V. Chandrasekar, and B. Cheong, 2014: A dual-polarization radar hydrometeor classification algorithm for winter precipitation. *J. Atmos. Oceanic Technol.*, **31**, 1457–1481, doi:10.1175/JTECH-D-13-00119.1.

Thurai, M., V. Bringi, M. Szakáll, S. Mitra, K. Beard, and S. Borrmann, 2009: Drop shapes and axis ratio distributions: Comparison between 2D video disdrometer and wind-tunnel measurements. *J. Atmos. Oceanic Technol.*, **26**, 1427–1432, doi:10.1175/2009JTECHA1244.1.

Tong, M., and M. Xue, 2005: Ensemble Kalman filter assimilation of Doppler radar data with a compressible nonhydrostatic model: OSS experiments. *Mon. Wea. Rev.*, **133**, 1789–1807, doi:10.1175/MWR2898.1.

Ulbrich, C. W., and D. Atlas, 1982: Hail parameter relations: A comprehensive digest. *J. Appl. Meteor.*, **21**, 22–43, doi:10.1175/1520-0450(1982)021<0022:HPRACD>2.0.CO;2.

——, and ——, 1984: Assessment of the contribution of differential polarization to improved rainfall measurements. *Radio Sci.*, **19**, 49–57, doi:10.1029/RS019i001p00049.

Wainwright, C. E., D. T. Dawson, M. Xue, and G. Zhang, 2014: Diagnosing the intercept parameters of the exponential drop size distributions in a single-moment microphysics scheme and impact on supercell storm simulations. *J. Appl. Meteor. Climatol.*, **53**, 2072–2090, doi:10.1175/JAMC-D-13-0251.1.

Wu, B., J. Verlinde, and J. Sun, 2000: Dynamical and microphysical retrievals from Doppler radar observations of a deep convective cloud. *J. Atmos. Sci.*, **57**, 262–283, doi:10.1175/1520-0469(2000)057<0262:DAMRFD>2.0.CO;2.

Xiao, Q., and J. Sun, 2007: Multiple-radar data assimilation and short-range quantitative precipitation forecasting of a squall line observed during IHOP_2002. *Mon. Wea. Rev.*, **135**, 3381–3403, doi:10.1175/MWR3471.1.

Xue, M., D. Wang, J. Gao, K. Brewster, and K. K. Droegemeier, 2003: The Advanced Regional Prediction System (ARPS), storm-scale numerical weather prediction and data assimilation. *Meteor. Atmos. Phys.*, **82**, 139–170.

——, M. Tong, and K. K. Droegemeier, 2006: An OSSE framework based on the ensemble square root Kalman filter for evaluating the impact of data from radar networks on thunderstorm analysis and forecasting. *J. Atmos. Oceanic Technol.*, **23**, 46–66, doi:10.1175/JTECH1835.1.

——, F. Kong, K. W. Thomas, J. Gao, Y. Wang, K. Brewster, and K. K. Droegemeier, 2013: Prediction of convective storms at convection-resolving 1-km resolution over continental United States with radar data assimilation: An example case of 26 May 2008 and precipitation forecasts from spring 2009. *Adv. Meteor.*, **2013**, 259052, doi:10.1155/2013/259052.

——, M. Hu, and A. D. Schenkman, 2014: Numerical prediction of the 8 May 2003 Oklahoma City tornadic supercell and embedded tornado using ARPS with the assimilation of WSR-88D data. *Wea. Forecasting*, **29**, 39–62, doi:10.1175/WAF-D-13-00029.1.

Zhang, G., M. Xue, Q. Cao, and D. Dawson, 2008: Diagnosing the intercept parameter for exponential raindrop size distribution based on video disdrometer observations: Model development. *J. Appl. Meteor. Climatol.*, **47**, 2983–2992, doi:10.1175/2008JAMC1876.1.

Zhang, J., 1999: Moisture and diabatic initialization based on radar and satellite observation. Ph.D. thesis, University of Oklahoma, 194 pp.

——, F. Carr, and K. Brewster, 1998: ADAS cloud analysis. *12th Conf. on Numerical Weather Prediction*, Phoenix, AZ, Amer. Meteor. Soc., 185–188.

Zhao, K., and M. Xue, 2009: Assimilation of coastal Doppler radar data with the ARPS 3DVAR and cloud analysis for the prediction of Hurricane Ike (2008). *Geophys. Res. Lett.*, **36**, L12803, doi:10.1029/2009GL038658.

Zrnić, D. S., and A. V. Ryzhkov, 1996: Advantages of rain measurements using specific differential phase. *J. Atmos. Oceanic Technol.*, **13**, 454–464, doi:10.1175/1520-0426(1996)013<0454:AORMUS>2.0.CO;2.

——, and ——, 1999: Polarimetry for weather surveillance radars. *Bull. Amer. Meteor. Soc.*, **80**, 389–406, doi:10.1175/1520-0477(1999)080<0389:PFWSR>2.0.CO;2.